Spring 2018

Multiscale approaches toward advanced lithium-ion battery: From nano to meso scale

Susmita Sarkar

Department:

MULTISCALE APPROACHES TOWARD ADVANCED LITHIUM-ION BATTERY: FROM NANO TO MESO SCALE

by

SUSMITA SARKAR

A THESIS

Presented to the Faculty of the Graduate School of the

MISSOURI UNIVERSITY OF SCIENCE AND TECHNOLOGY

In Partial Fulfillment of the Requirements for the Degree

MASTER OF SCIENCE IN MECHANICAL ENGINEERING

2018

Approved by

Jonghyun Park, Advisor
Heng Pan
Fatih Dogan

PUBLICATION THESIS OPTION

This thesis consists of the following three articles which have been published, or will be submitted for publication as follows:

Paper I, Pages 8-35 was published in ACS APPLIED MATERIALS & INTERFACES, 2017, 9, (36), 30599-30607

Paper II, Pages 36-58 is intended for submission in JOURNAL OF POWER SOURCES

Paper III, Pages 59-71 is intended for submission in NANO LETTERS

ABSTRACT

Battery performance and its degradation are determined by various aspects such as the transport of ions and electrons through heterogeneous internal structures composed of constituent particles, kinetic reactions at the interfaces, and a corresponding interplay between mechanical, chemical, and thermal responses. Further, modern battery materials require a variety of engineering processes such as coating, doping and mixing. As a result, in order to fully understand the behavior of the battery material and improve battery performance, it is necessary to understand and control the individual particle behavior and then connect it to the electrode. This study elucidated the physical phenomena associated with coating and grain boundaries and addressed the impact on cell-level performance. We also studied how to improve battery performance by changing the material and geometry of electrode components. The study was divided into three topics. First, it has been proved how an optimal layer thickness of CeO_2 layer by ALD is better than too think or too thick layer in terms of li-ion diffusion, transition metal-ion dissolution and mechanical damage. Second, it was shown that how grain boundary can improve the cell performance significantly. Grain-boundary possesses different diffusion co-efficient than the bulk and thus the performance is different than the electrodes where no grains are considered. Also, it was shown how grain boundary has impact on stress generation for both cathode and anode particles. Finally, an attempt has been made to use Ni-VO_x based nanofiber supported with carbon nanofiber to be used as an anode for advanced li-ion battery. Not only the process is simple but also the cell showed improved reversibility at a current rate of 100 mA/g.

ACKNOWLEDGMENTS

I would like to express my sincere appreciation and gratitude to my advisor, Prof. Jonghyun Park, for introducing me to this exciting field giving me an opportunity to do research in his laboratory. Without his constant support throughout the course of this research work, this thesis would have been impossible. I am grateful to him for the effort he put in, even outside regular office hours, to teach me and help me solve the problems, whenever I ran into any trouble or had questions about the research. I also gratefully acknowledge National Science Foundation (NSF) and University of Missouri Research Board (UMRB) for providing funds to carry out the research.

I wish to thank Prof. Heng Pan and Prof. Fatih Dogan for serving in my committee and taking their time to read my thesis and providing valuable insights which made the thesis a lot better than it was initially.

I wish to thank my lab mates Sindhuja Valluri, Yufang He, Jie Li, Hiep Pham and others whom I have worked along during my time at AEMS Lab and Xiaowei Yu from Prof. Pan's lab, for continuous support, technical discussions and understanding the topics.

I would also like to thank all my mother, father and sister for all the love and encouragement. They have always supported me, and I admire their sacrifice. I am thankful to have lots of good friends in Rolla and they have patiently extended all sorts of help for accomplishing this undertaking. I am very grateful to my cousin, sister-in-law and Bikram for all their help and support, from the day one of my graduate school.

TABLE OF CONTENTS

Page

LIST OF ILLUSTRATIONS

1. INTRODUCTION

With the mounting energy crisis from non-replenshible, dwindling fossil fuel sources, green energy sources such as solar, wind, hydroelectric power etc. are gaining paramount attention. However, unmanageable and sporadic nature of these renewable energy source, results in enormous demands of energy storage systems. Lithium Ion batteries are currently the cutting-edge energy storage devices. After the invention of first lithium based primary battery in 1912 by G.N.Lewis, engineers and scientists finally overcome the reactive characteristic of lithium metal and turned this into a secondary cell. In year 1991 Sony made first successful commercial version. Now, Li-ion battery occupies the majority of the battery market thanks to its unmatchable combination of high power and energy density. From Portable electronics such as phone, tablet to electric vehicles and NASA based aerospace missions, li-ion battery powers everything. Now, Lithium metal has been replaced by different types of electrode materials, making it more safe, reliable and reversible over several hundred cycles.

1.1 LITHIUM ION BATTERIES: PRINCIPLE AND OPERATION

As the name suggest, lithium-ion battery mainly relies on the repeated transfer of lithium ions to power up the devices. The lithium ion battery is made up of three active components: the cathode, the anode, and the electrolyte. Although the cathode and the anode are both referred to as electrodes and, in rechargeable batteries, switch depending on whether the battery is being charged or discharged, this work refers to the cathode and anode as static and defined by discharge.

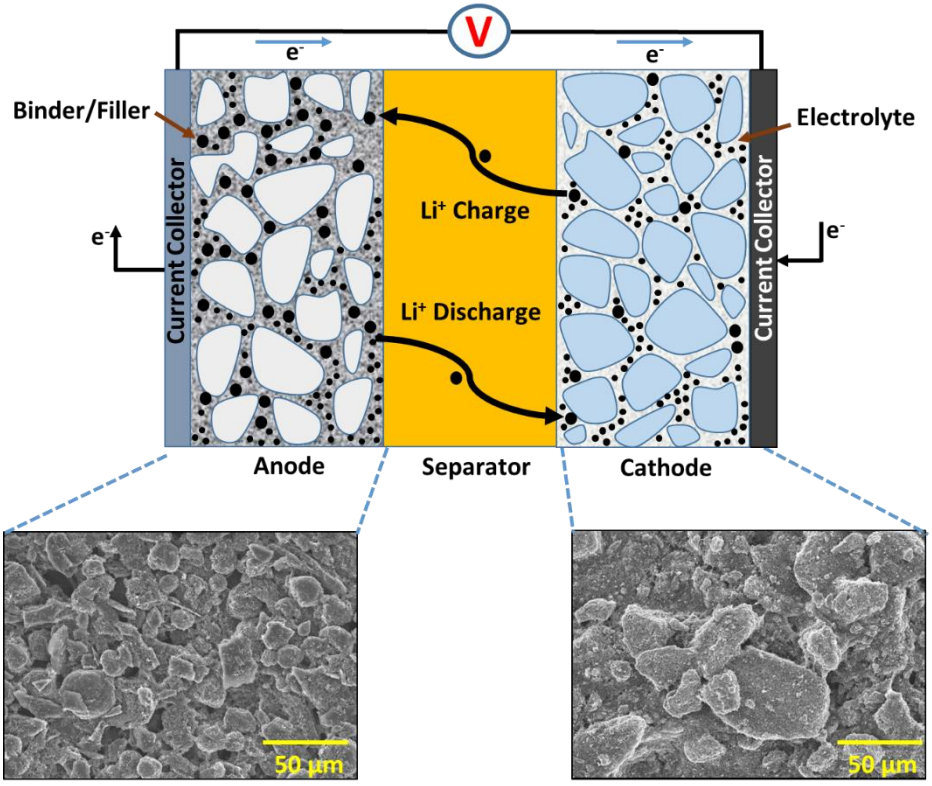

Figure 1.1. Schematic illustration of a lithium ion battery. The lower pictures in the figure are scanning electron microscope (SEM) images of different battery component materials. From left to right, a negative electrode using graphite as active particle materials and a positive electrode using $LiMn_2O_4$ active particles.

During discharge process, the anode, typically graphite, loses positively charged lithium ions to the electrolyte, freeing up electrons. The cathode, variable but typically a lithium compound, gains positive lithium ions from the electrolyte. The freed electrons from the anode side travel through the attached load to the cathode side in order to balance the newly created charge imbalance. On the other hand, while charging lithium ion travels from the cathode to the anode through the electrolyte. Both electrodes have current collectors, metallic conductors that attach the electrode to the outside electrical system, and can be thought of as the terminals of the battery. A charge balance is preserved in the cell through the continuous movement of li ions and electrons. For current Li-ion batteries,

some of the most common cathode materials are transition meal oxides (layered and spinel compounds), phosphates (olivine compounds) and Titanate such as $LiMn_2O_4$, $LiCoO_2$, $LiFePO_4$, $LiCoCO_2$, $LiCo_{1/3}Mn_{1/3}Ni_{1/3}O_2$ etc., while graphite is the much used anode material.[1–5] The electrochemical redox reactions of Graphite/$LiMO_2$ (M= Mn, Ni, Co etc.) system are described below:

- Negative electrode: $Li_xC_6 \rightarrow C_6 + xLi^+ + xe^-$ (anodic reaction; oxidation)
- Positive electrode: $Li_{1-x}MO_2 + xLi^+ + xe^- \rightarrow LiMO_2$ (cathodic reaction; reduction)
- Overall reaction: $Li_xC_6 + Li_{1-x}MO_2 \rightarrow LiMO_2 + C_6$

The electrodes also have additional non-reacting elements, such as carbon black, to enhance electron transport to and from the current collector as well as a binding agent to maintain cohesive macro-structure and ensure electrical contact. The part of the electrode that interacts with the lithium ions is more specifically called the active material, and consists of multiple nanoparticles. In addition, there is a non-participating solid but porous separator between the two electrodes. This is here to prevent any electrical contact between electrodes, as metallic lithium ion far-reaching dendrites can form on the electrode surface and could risk an electrical short in the system if left unguarded.

1.2. DEGRADATION MECHANISM OF LI-ION BATTERIES

Yet looking to the future, the usefulness of li ion batteries to power the ever-growing world's needs are treated with skepticism. Li-ion batteries suffer from several degradations depending upon the material chemistry. Although intercalation type of cathode materials are the much popular one because its framework guarantees the cell chemistry reversibility. However, their stationary lattice structure can mostly

accommodate on Li per transition metal, giving much less li intercalation capacity. These intrinsic limits can be overcome by using the conversion-reaction materials. Conversion-reaction materials undergo a conversion reaction with lithium and often accommodate more than one Li atom per transition-metal cation: [6]

$$M_aX_b + (b.n)Li^+ \leftrightarrow aM + bLi_nX \quad (1)$$

(M= Ni, Mn, Fe, Co, Ni, Cu, Cr etc., X=O, F, N, S, P, H, etc. and n is the oxidation state of X). Even though these materials always shuttles multi-ions and possess remarkable specific capacities, the challenges like low electronic conductivity, voltage hysteresis and volume expansion during charging/discharging limits the rate capability, decays the capacity, hinders cycling stability and causes the low energy efficiency.

Currently the most commonly used anode materials are based on graphite and lithium alloyed metals. Graphite based materials consist of sheets packed in hexagonal (AB) or rhombohedral (ABC) arrangements.[7] Upon lithium ion insertion, graphene staging occurs where the graphene sheets stacked themselves in AA arrangement. Despite several advantages such as abundance, minimal cost and suitable electrochemical properties, graphite carbon shows poor lithium intercalation capacity compared to Li alloy anodes. Thus graphite material suffers from high irreversible capacity loss, lithium dendrite formation etc. Lithium-metal alloys (M= Al, Mg, Sn, Sb etc.) showed excellent intercalation capacity. However, this alloys suffered from high volumetric change during li insertion/de-insertion, causing the cycling instability over time. $Li_4Ti_5O_{12}$ have emerged as a potential anode material as it has higher rate capability, cycling stability and structural stability due to lower volumetric change (less than 0.2%).[8] However, its high operating voltage and low capacity restricted its use to only low energy density applications. Also,

significant research has been done on the metallic element based such as Si and Sn based materials as high capacity anode materials.[9–12] Despite extremely high capacity at initial cycle, these materials loses the capacity significantly with time and the main culprit is enormous volume change during li intercalation/de-intercalation, shattering the structural integrity. Several efforts on industrial and academic levels are underway looking for inter-metallic composite anodes with high capacity and cycling stability.

1.3. CELL ELECTRODES: IMPORTANCE AND IMPROVEMENT

The physical and chemical properties of the electrode material influences the overall battery performance and thus must be reviewed and used appropriately. Unwanted intrinsic chemistry and inherent defects the raw material causes the less capacity utilization. Along with material selection, convenient skeletal modifications are necessary for improved cell performance.

1.3.1. Improvement of Electrodes Particle via Coating. Advances in the li-ion battery cycling performance has been achieved by the deposition of nano-coating layer on surface of another nanoparticles. Several deposition techniques such as Chemical vapor deposition, Pulsed laser deposition, Sputtering and Atomic layer deposition (ALD) has been thoroughly researched. ALD is a much popular method to deposit conformal, pinhole free ultra-thin films on complex electrode substrates. The lithiated cathode materials such as $LiMn_2O_4$, $LiCoO_2$, $LiFePO_4$ and unlithiated transition metal oxides such as TiO_2, Co_3O_4, V_2O_5, ZrO_2, Al_2O_3, CeO_2, NiO, Fe_3O_4, MnO_2, SnO_2 etc. are some of the electrode material that has been used for ALD coating.[13–25]

1.3.2. Grain Boundary Induced Improvement in Electrode Particles. The synthesizing method influences the micro-morphology of electrode structure by changing the crystallinity atomic order, thus causing the different electrochemical performances of the same electrode material. Grain boundaries affects the material electro-mechanical properties to a large extent. For the battery material, lithium ion conducting behaviors will largely depend on the electrode microstructures such as density, domain boundaries and atomistic structures. All these structural factors will significantly contribute to the overall conductivity of the material.[26–32]

1.3.3. Structural Improvement of Electrodes. Modification of electrode architectures brings good li-ion cell capacity retention without damaging the host structure. 0D structures-nanoparticles, 1D structures-nanowires, nanofibers and nanotubes, 2D structures-layered material and 3D structures-mesoporous structures are the commonly researched electrodes.[33–36] Nanoparticles shorten the li ion diffusion paths and also, lessens the mechanical damage during li insertion/de-insertion and thus, improving the cycling performance. 1D structures possess all the benefits of nanoparticles and also, has higher surface area to volume ratio for the electrode-electrolyte interfaces, efficiently transports the electrons along the longitudinal direction. 2D materials such as graphene and MoS_2 are very thin and thus exhibits instantaneously accessible electrochemically active sites. 3D structures with high mesopores and high surface area leads to efficient electrolyte penetration throughout the electrode material, improving the capacity retention and cycling stability significantly.

2. SCOPE AND OBJECTIVE

In the first part, a multiphysics-based model which takes into consideration stress mechanics, diffusion of lithium ion, and dissolution of transition metal ions of spinel $LiMn_2O_4$ cathode is reported. The model analyzes how different CeO_2 coating thicknesses affect diffusion-induced stress generation and, ultimately, crack propagation. Experimentally measured diffusivity and dissolution rates were incorporated into the model to account for a trade-off between delayed transport and prevention of side reactions

In the second particle-level model has been developed which incorporates the grain boundary diffusion in the electrode particles for the anode and cathode electrodes. The developed model is compared against the grain-less model at various operating conditions to understand how grain boundaries influence capacity and stress generation in Li ion batteries.

In the third part, synthesis of carbon supported flexible Nickel wrapped vanadium oxide electrodes for high performance li-ion battery is reported. The electrode will be used as it is without the need of extra binders and conductive agents. Cyclic performances of bare, 3wt% Ni added and 5 wt% Ni added VO_x CNF has been examined and it was shown how the amount of Ni matrix has a significant impact on overall cell performance and cycling stability.

PAPER

I. UNVEILING THE ROLE OF CEO_2 ATOMIC LAYER DEPOSITION COATINGS ON $LIMN_2O_4$ CATHODE MATERIALS: AN EXPERIMENTAL AND THEORETICAL STUDY

Susmita Sarkar[1], Rajankumar L. Patel[2], Xinhua Liang[2], Jonghyun Park[1,*]

[1]Department of Mechanical Engineering, Missouri University of Science and Technology, Rolla, MO 65409, United States

[2]Department of Chemical and Biochemical Engineering, Missouri University of Science and Technology, Rolla, MO 65409, United States

*Corresponding author Email: parkjonghy@mst.edu

ABSTRACT

An Atomic Layer Deposition (ALD) coating on active materials of a lithium ion battery is a more effective strategy for improving battery performance than other coating technologies. However, substantial uncertainty still remains about the underlying physics and role of the ALD coating in improving battery performance. Although improvement in the stability and capacity of CeO_2 thin film coated particles for batteries has been reported, a detailed and accurate description of the mechanism has not been provided. We have developed a multiphysics-based model which takes into consideration stress mechanics, diffusion of lithium ion, and dissolution of transition metal ions of spinel $LiMn_2O_4$ cathode. The model analyzes how different coating thicknesses affect diffusion-induced stress generation and, ultimately, crack propagation. Experimentally measured diffusivity and

dissolution rates were incorporated into the model to account for a trade-off between delayed transport and prevention of side reactions. Along with experimental results, density functional theory results are used to explain how a change in volume, due to dissolution of active material, can affect battery performance. The predicted behavior from the model is well matched with experimental results obtained on coated and uncoated $LiMn_2O_4$-Li foil cells. The proposed approach and explanations will serve as important guidelines for thin film coating strategies for various battery materials.

Keywords:

Lithium Ion battery, ALD coating, battery degradation model, Lithiation-induced stress, Mn dissolution

1. INTRODUCTION

Lithium-Ion Batteries (LIBs) are used in a variety of applications, including portable devices and transportation/stationary applications. However, their cycle performance cannot keep pace with ever-burgeoning consumer demand. Besides developing new electrode materials, surface coatings have been scientifically proven [1–3] to be a budgetary and attainable technology that can overcome a poor cycle lifetime. Through the process of making thin wall on a Sb hollow yolk,[4] embedding NiSb alloy in carbon hollow spheres,[5] and by the formation of hierarchical Fe3O4@PPy nanocages[6], high capacity and extreme cycling stability has been achieved for Li-ion batteries. However, the understanding of surface coating physics and its functionalities is still in its infancy, and is critical to the development of next generation LIBs. Despite numerous reports of surface coatings, such as sol-gel[7–9] and CVD techniques,[10],[11]

these are not suitable for nanoscale applications due to a lack of control of surface thickness, consistency, and conformity. Atomic Layer Deposition (ALD) has proven to be the best method for depositing continuous and conformal films.[12–14] The ALD process is based on sequential self-limiting, non-overlapping, and self-saturating surface reactions, so it can be employed to deposit defect-free, conformal atomically thin layers.[15–17] These layers then act as protective barriers to improve battery life and prevent degradation, even with elevated temperatures and fast cycle rates. Maximum initial capacity and capacity retention for a long cycle life for LIBs have been examined by applying various coating materials (such as AlF_3,[18–21] Al_2O_3, [22,23] MgO,[24] SiO_2,[25,26] ZrO_2,[27,28] and $TiO_{2)}$,[29] while the coating thickness subsequently changed from a sub-micrometer range to a nanometer range. Recently, the authors demonstrated that an optimized CeO_2 film (~ 3 nm), coated with $LiMn_2O_4$ particles, exhibited a significant improvement in capacity and cycling performance, as compared to uncoated, Al_2O_3 coated, and ZrO_2 coated samples at room temperature, and at 55 °C for long cycling numbers (1,000 cycles).[30]

So far, the proposed mechanisms that explain performance improvement, via coating strategy, can be summarized as follows. First, cell voltage rapidly drops at high currents due to the semiconducting or insulating properties of electrode materials. Here, a thin layer of conductive material on the surfaces of electrodes can provide fast electrons by reducing interfacial resistance.[31] Moreover, when the operating voltage of a cathode exceeds the electrolyte oxidation, the cathode intensifies the decomposition of the electrolyte. The produced hydrofluoric acid (HF) dissolves transition metal ions and erodes the surfaces of the active materials. In this case, the coating not only slows down surface

corrosion, but also retards the gradual surface oxidation of low-valent active materials (such as $LiFePO_4$ and VO_2).[32–35] Additionally, coating layers can act as flexible shells to accommodate volume expansions and contractions of active materials during Li intercalation/de-intercalation.[36]

Despite the fact that several researchers have identified the beneficial roles of electrode coating, only a few reports have been published concerning weighable features of surface coating techniques based on comprehensive and quantitative analyses. A few studies have been reported that focus on the transport of lithium ions through some insulating or semi-conductive coating materials. For Al_2O_3 coating, $Li_{3.4}Al_2O_3$ was found to be the most energetically suitable structure of lithiated alumina, as lithium ion diffusivity was higher in the optimal concentration than in the diluted Li concentration.[37] An ohmic electrolyte model that assumed electrical insulation, but ionic conductivity of many ideal coatings (α-AlF_3, α-Al_2O_3, m-ZrO_2, c-MgO, and α-quartz SiO_2), predicted a lithium diffusion coefficient and solubility in those coating materials.[38] The passivation properties of the coating materials on electrode surfaces were investigated through first-principles calculation. This revealed how an ALD coating could better retard the electron transfer process in electrolytes and reduce solvent decomposition, as compared to bare electrodes.[39] However, atomistic-level studies of coating properties have been inadequate in accounting for measurable improvements in battery performance or irreversible capacity loss. Further, scattered reports in the literature have investigated the underlying properties of coatings by mainly focusing on the diffusion properties of lithium ion.

This paper reports a comprehensive and quantitative understanding of the intrinsic properties of the ALD-coated active materials. Figure 1 depicts (a) a CeO_2-ALD thin film coated cathode particle and (b) a half-cell containing positive electrode materials enveloped by a uniform CeO_2 thin film.

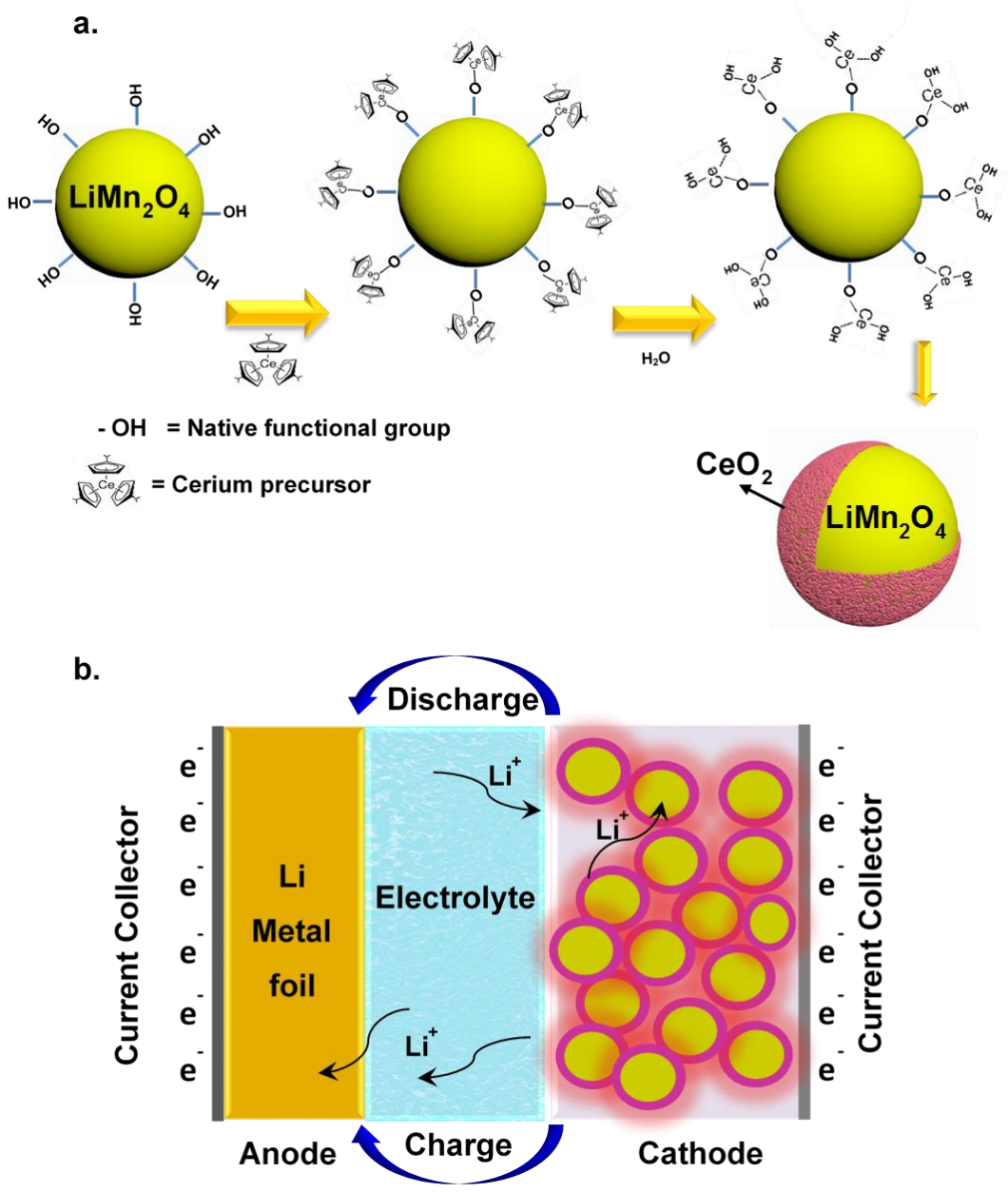

Figure 1. **(**a) Illustration of CeO_2 based ALD coating on $LiMn_2O_4$ particle; (b) Schematic showing transportation of ions inside the li ion battery. Coating allows the faster movement of Li^+ ions but delays the transition metal ion (Mn^{3+}) diffusion.

To explain the behavior of Li diffusion, stress generation, and metal ion dissolution, a coupled mechanical-electrochemical model (based on a single particle) was developed. Based on the authors' published diffusivity measurements,[40] the coating thickness-dependent electronic and ionic conductivity effects were investigated here. The trade-off impacts of coating thickness on mechanical stability, transfer delay, and side reaction prevention were satisfactorily explained via the developed Multiphysics model. Further, first-principle calculations were used to compare the estimated volume changes of the active materials (due to dissolution) from the measured and literature values. Results from the Finite Element Method (FEM) simulation and experimental observations showed a general consistency with the Density Functional Theory (DFT) simulation outcome. The predicted capacities of uncoated and coated particles were similar to the experimental results,[30] indicating appropriate assumptions for the proposed mechanisms and multiple input parameters. These combined results shed light on the fundamental physical mechanism of an ALD-coated electrode in relation to its inherent electrochemical status.

2. COMPUTATIONAL METHODS

A single $LiMn_2O_4$ (LMO) particle, uncoated or coated with different thicknesses, was considered in the model to simplify the system without including binders and conductive agents, as in the references.[41],[42] This model assumed that the cathode particles were homogeneous, isotropic, and single-phase spherical particles. Considering the symmetry boundary conditions, ½ geometry was employed, as shown in Figure 2, to improve computational efficiency.

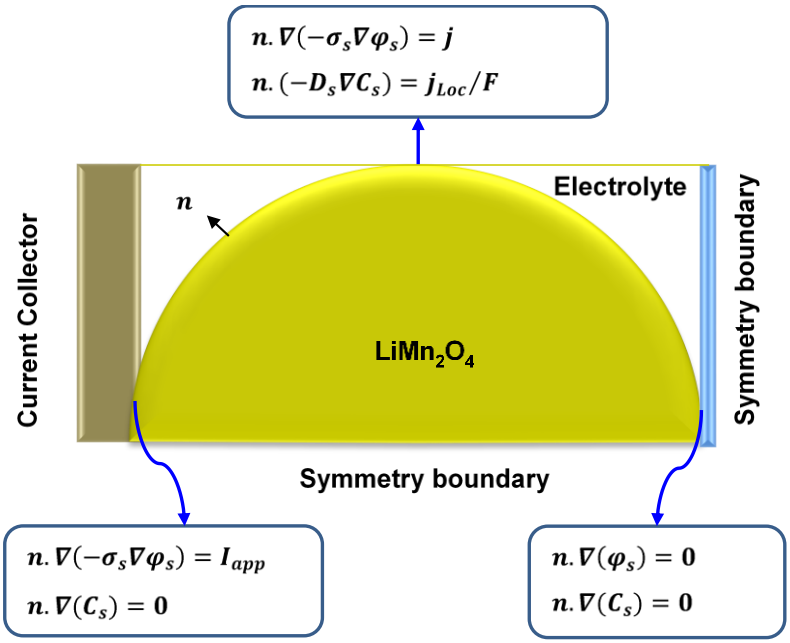

Figure 2. $LiMn_2O_4$ particle, representing interface boundary conditions. ½ Geometry was utilized considering the symmetry boundary condition. At the cathode and electrolyte interface, electric potential and li flux is governed by charge-transfer reactions. At symmetry boundaries, both electronic and li flux must disappear. The charge/discharge current is specified at current collector and cathode interface.

In this model, three key physics were integrated:

(1) The intercalation of lithium ions creates stress in the particles, which can lead to cracking. The generation of stresses and the stress-strain relationship with the concentration gradient in an isotropic media can be written as

$$\varepsilon_{ij} = \frac{1}{E}\left[(1+\gamma)\sigma_{ij} - \gamma\sigma_{kk}\delta_{ij}\right] + \frac{\Delta C_s \Omega}{3}\delta_{ij} \quad (1)$$

Where ε_{ij} and σ_{ij} represent strain and stress components, respectively. E is Young's modulus, γ is Poisson's ratio, δ_{ij} is Kronecker delta, Ω is the partial molar volume of solute, and ΔC_s is the concentration change of the diffusion species from the original value. The stress value is coupled with the diffusion problem using the following equation,

$$-D\left(\nabla c_s - \frac{\Omega c_s}{RT}\nabla\sigma_h\right)\cdot n = \frac{i_n}{F} \quad (2)$$

Where σ_h is the hydrostatic stress. (2) The electronic and ionic transport considering mass and charge balances in the electrolyte and solid phases. For example, mass balance and charge balances in the solid phase are given by

$$\frac{\partial c_s}{\partial t} = \frac{1}{r^2}\nabla.(r^2 D_s \nabla c_s) \quad (3)$$

$$\nabla(-\sigma_s \nabla\varphi_s) = 0 \quad (4)$$

Where C_s is the concentration of lithium at the surface of the sphere for a cathode, D_s is the diffusion coefficient of lithium in the solid phase, σ_s is the solid phase conductivity, and ϕ_s is the local potential for an electrode.

(3) Mn dissolution and the corresponding side effects that include solvent oxidation, electrolyte decomposition, and hydrogen reduction reaction. For example, the current density due to electrolyte oxidation is given by

$$j_{oxide} = a_c i_0^{sol}\left\{exp\left[\frac{\alpha_a^{sol}}{RT}F\eta_{oxide}\right] - exp\left[-\frac{\alpha_c^{sol}}{RT}F\eta_{oxide}\right]\right\} \quad (5)$$

Where $\eta_{oxide} = \phi_s - \phi_e - U_{oxide}^{eq}$ and a_c is the surface area per unit volume for solvent oxidation. Another important effect of dissolution is the volume fraction change and particle connectivity change that result in effective transport properties. These effective transport properties are described by Bruggeman's relation that utilizes the volume fraction of each material phase as[43],[44]

$$D_{Li+}^{eff} = D_{Li+}^{0}\left[1 - \left(\frac{\varepsilon_{pos0} - \varepsilon_{pos}}{\varepsilon_{pos0}}\right)^{n_1}\right] \quad (6)$$

$$k^{eff} = (\varepsilon_e)^{1.5} k_e \quad (7)$$

$$\sigma^{eff} = (\varepsilon_e)^{1.5} \sigma_s \quad (8)$$

Where D_{Li+}^{0} is the initial diffusion coefficient, n_1 is the adjustment factor for the diffusion coefficient of lithium ions in the electrolyte, and k_e and σ_s are the initial ionic and electronic conductivity of the electrolyte and solid phase, respectively. All necessary equations are given in the supporting information (Table S1, S2, and S3).

Calculation of the model was performed using COMSOL MULTIPHYSICS®. One important phenomenon of Mn dissolution is volume change and the corresponding effective property changes and contact loss. Density Functional Theory (DFT) calculations were used to measure the exact volume change due to Mn dissolution. The GGA (Perdew−Burke−Ernzerhof (PBE) exchange and correlation function),[45] with the projector augmented wave (PAW)[46] method, were as implemented in the Vienna *ab initio* simulation package (VASP).[47] A 3×3×3 mesh of k points was used to sample the Brillouin zone. Energy cutoff of the plane waves was chosen to be 780 eV (1.3×600 eV). A relaxation process was carried out, including geometry minimization of the atomic positions, per inter-atomic forces.

3. EXPERIMENTAL SETUP

ALD coating of ultrathin CeO_2 on $LiMn_2O_4$ (LMO) powders was done by following the procedure described previously[30]. Briefly, a fluidized bed reactor was used to perform ALD to coat various thicknesses of CeO_2 thin films on LMO powders, at 250°C, using two reactant chemicals: tris(ipropylcyclopentadienyl) cerium ($Ce(iPrCp)_3$) (99.9%,

Strem Chemicals) and de-ionized water. Next, cathodes were prepared using different coated LMO powders (Polyvinyldebe fluoride (PVDF), Carbon black (CB), and N-Methyl-2-pyrrolidone (NMP)) in the conventional slurry method. The load mass of uncoated electrode and 3nm coated electrode was 2.9 mg and 3.7 mg, respectively. Lithium foils served both as a counter electrode and as a reference electrode. The commercial electrolyte, composed of $LiPF_6$ dissolved in a mixed solvent of EC: DMC: DEC (1:1:1), was used. Finally, a cell was assembled into a CR2032 coin cell format.

To examine the crack evolution in the electrodes, the uncoated (UC) LMO cell was cycled for 800 times at 1C at room temperature (RT). It was kept for about 1 year before it was opened. A 3 nm coated (3nm-Ce) LMO cell was cycled for 1,003 times at 1 C-rate, RT, and kept for about 1 year, before opening. All of the cathodes were cleaned with acetonitrile and ethanol before examination by SEM.

For the dissolution experiment, one batch of the UC LMO and 3nm-Ce LMO particles was soaked in electrolyte for 5 weeks, at RT, in an Ar-filled glove box, and then the powders were washed with dimethyl carbonate (DMC) to remove traces of electrolyte. Then, an Inductively Coupled Plasma - Optical Emission Spectrometry (ICP-OES) analysis was used to confirm the amount of dissolved transition metal in the electrolyte solution left, after removal of the contained powder.

For conductivity measurement, pellets of UC, 2 nm coated (2nm-Ce), 3 nm coated (3nm-Ce), and 5 nm coated (5nm-Ce) particles were prepared. An IviumStat impedance analyzer was used to obtain impedance curves at 1 mHz – 1 MHz frequency range. Testing was done at a range of 0.2 V to 1.4 V, and the corresponding current was tracked after 60

s of stabilization time at each step. This experimental procedure is like the conductivity experiments performed in our recent report.[40]

From the experimentally obtained ionic conductivities for uncoated (UC) and coated particles, the diffusion coefficient were evaluated based on the generic relationship between diffusivity (D_i) and ionic conductivity (σ) given by[48]

$$\sigma = \frac{q_i^2 c_i}{K_B T} D_i \tag{9}$$

Where q_i is the charge of the solute i in C, K_B is the Boltzmann constant, and T is the temperature.

4. RESULTS AND DISCUSSION

To understand the impact of ALD, it is vital to ascertain how the ionic and electronic diffusivities of the coated particles differed from those of the uncoated active materials in Li-ion batteries. Diffusion in crystal and polycrystalline solid state materials can involve surface diffusion, bulk diffusion, lattice diffusion, and grain boundary diffusion. Due to the high concentration of defects in the grain-contact area, resulting from their crystallographic misalignment, grain boundary diffusions were much faster than in bulk, but slower than in the boundary between the solid and air (surface diffusion). ALD films are very thin (few nm) and generally amorphous, so the surface diffusion was dominant. As evidence, Figure 3 shows the diffusion coefficient as a function of coating thickness, evaluated based on the relationship between the experimentally obtained conductivity and diffusion coefficient. At thicknesses below 3 nm, the diffusion coefficient

increased with increasing thickness while, at thicknesses above 3 nm, the diffusion coefficient decreased with increasing thickness.

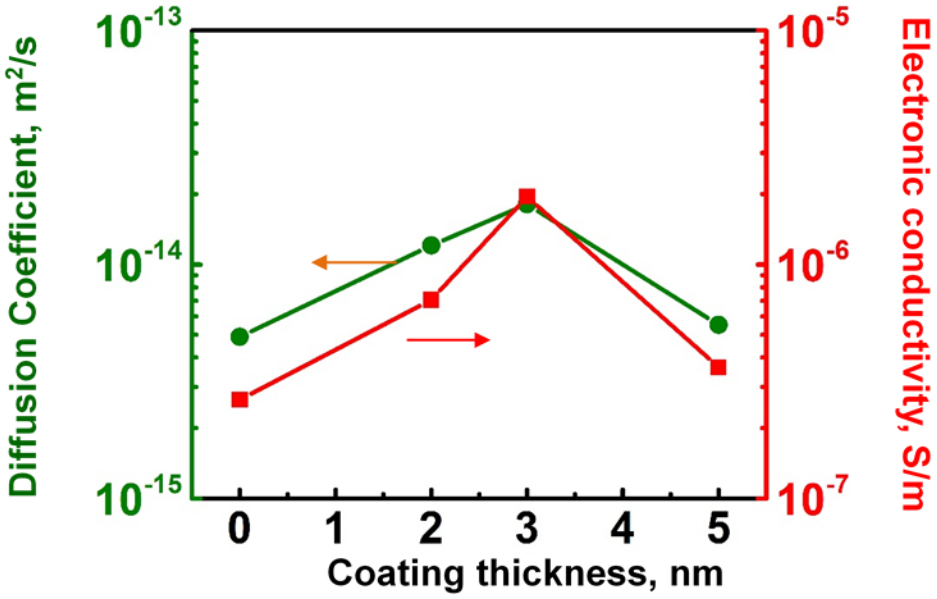

Figure 3. Diffusion Coefficient and Electronic Conductivity as a function of CeO_2 coating thickness

A similar observation was reported[49] in which lithium ion diffusion in $CeO_2 \cdot TiO_2$ thin film was investigated. It was found that there were three regions, including a fast lithium ion diffusion region below 100 nm, a slow diffusion region, and a fast diffusion region above 150 nm. Electronic conductivity was also found to follow the same pattern of diffusivity. Due to the crystal orientation, LMO was shown to have semiconducting properties.[50] Conductivity increased for the samples with up to 3 nm and then began to decrease. The conductivity of the 3nm coated particles was nearly one order of magnitude higher than the conductivity of the uncoated LMO. This improvement can be attributed to the formation of ion transport channels between the electrode and the coating, which enhanced ion diffusion into the LMO through the entire surface.[51]

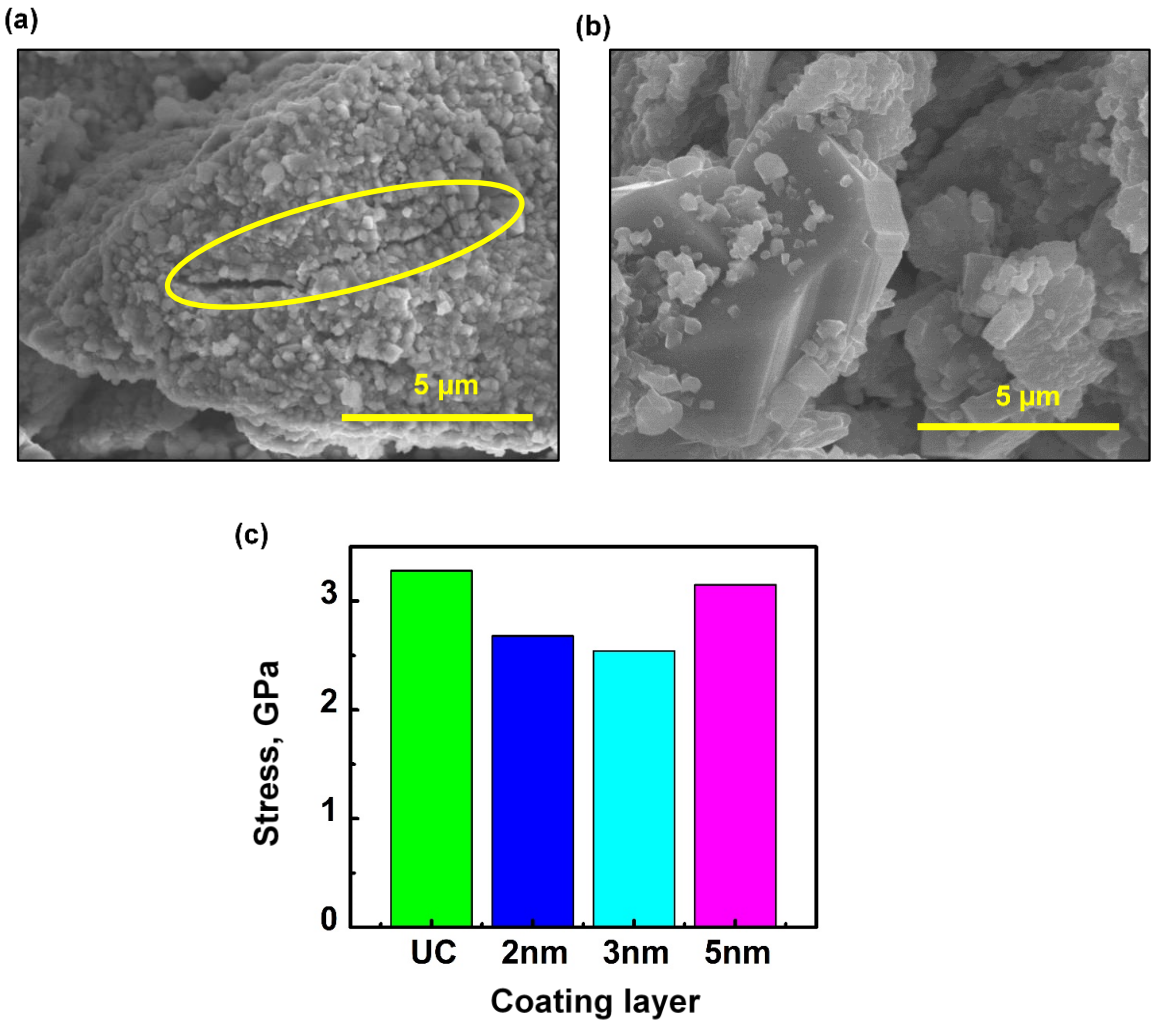

Figure 4. SEM images of (a) UC after 800 charge-discharge cycles at room temperature; (b) 3nm-Ce after 1000 charge-discharge cycles at room temperature. Clearly, the cracks are visible in the UC sample after cycling, while the 3nm-Ce sample showed almost no cracks. (c) Stresses for different coating layer thickness. UC LMO particles has the maximum principle stress.

Crack propagation and fracture are important capacity fading mechanisms in modern LIBs. During the lithium intercalation in active materials, volume changes and phase transformations instigate different stresses[52,53] which, in turn, create crevices along the phase boundaries[53] of the active materials. Critical values of tensile and compressive stresses promote microscopic fractures and cause structural failure of

electrodes.[54] Experimental and theoretical studies of bare and coated particles were conducted to examine and determine the mechanical stability of electrode materials with ALD. Figures 4(a) and 4(b) show SEM images of cathode particles after charge and discharge cycling. Figure 4(a) shows an UC LMO sample after 800 charge-discharge cycles at 1C, at room temperature, and figure 4(b) shows a 3nm coated LMO sample after 1,000 cycles under same conditions. As shown in the figures, the bare and coated LMOs initially exhibited no fracture. However, after 1000 cycles, in the case of the bare particles, cracks appeared to begin on the outer surfaces of the particles propagating inside the core. Cracks could be clearly seen throughout all of the entire uncoated particles. These cracks were evident on almost all uncoated particles that were analyzed using SEM, while the 3nm coated LMO sample showed no cracks, even after 1,000 charge-discharge cycling. SEM inspection was carried out at about the same time, duration, and under the same conditions as the UC samples, so visible cracks of the 3nm-Ce LMOs would not be missed. A numerical model was developed to quantitatively analyze stress evolution inside the particle and correlate it with degraded battery performance. The key purpose of this model was to interpret the maximum principle stresses detected with and without ALD coatings. This model was based on a previous study[55], which considered Li diffusion in a phase changing (cubic to tetragonal phase) intercalation material. The model was reformulated by neglecting the phase change and examining the dependence of stress evolution on the coating thickness. This showed that uncoated particles had the highest stress that was reduced as the coating layer thicknesses increased. Figure 4(c) summarizes the value of stresses on the uncoated and coated particles. This mechanical stress is the driving force behind the experimentally observed crack propagation. Crack propagation is accelerated in

the bare LMO compared with ALD-coated LMO, suggesting that an ALD coating can help arrest crack penetration. Thus, it can be concluded that 3 nm coated particles effectively interfere with crack propagation. This crack propagation should be related to the dissolution of active materials, which is another major intrinsic degradation mechanism in LIBs, as it creates more interfaces with the electrolyte.

Degradation of active materials is a process through which transition metal ions dissolve in electrolyte.[56] It has been established that, in stress corrosion cracking, when an uncovered metal surface was exposed to a hostile environment, loss of dissolved metal ions led to the formation of gaps and cracks.[57] With a continuous cycle of material dissolution, crack propagation was promoted further.[58,59] In LIBs, the presence of corrosive Hydrofluoric acid (HF) in electrolyte, accelerated the dissolution and led to a significant loss of capacity upon cycling.[60,61] A common approach to suppressing HF content was the application of protective coatings of binary oxides on cathode particles. A double shell $LiMn_2O_4$@$LiNi_{0.5}Mn_{1.5}O_4$ combined with an interior void can effectively suppress the Mn ion dissolution at the surface and shows unique rate capability and cycling stability.[62] However, the proper relationship between coating materials and transition metal loss is not clearly understood to date. This work has incorporated the complex nature of side reactions between the cathode, coating, and electrolyte, and effective performances have been observed. As proven in the literature, capacity fading during cycling is commonly linked to manganese dissolution into the electrolyte solution and, thus, the solubility of coated and uncoated LMOs was examined at room temperature.

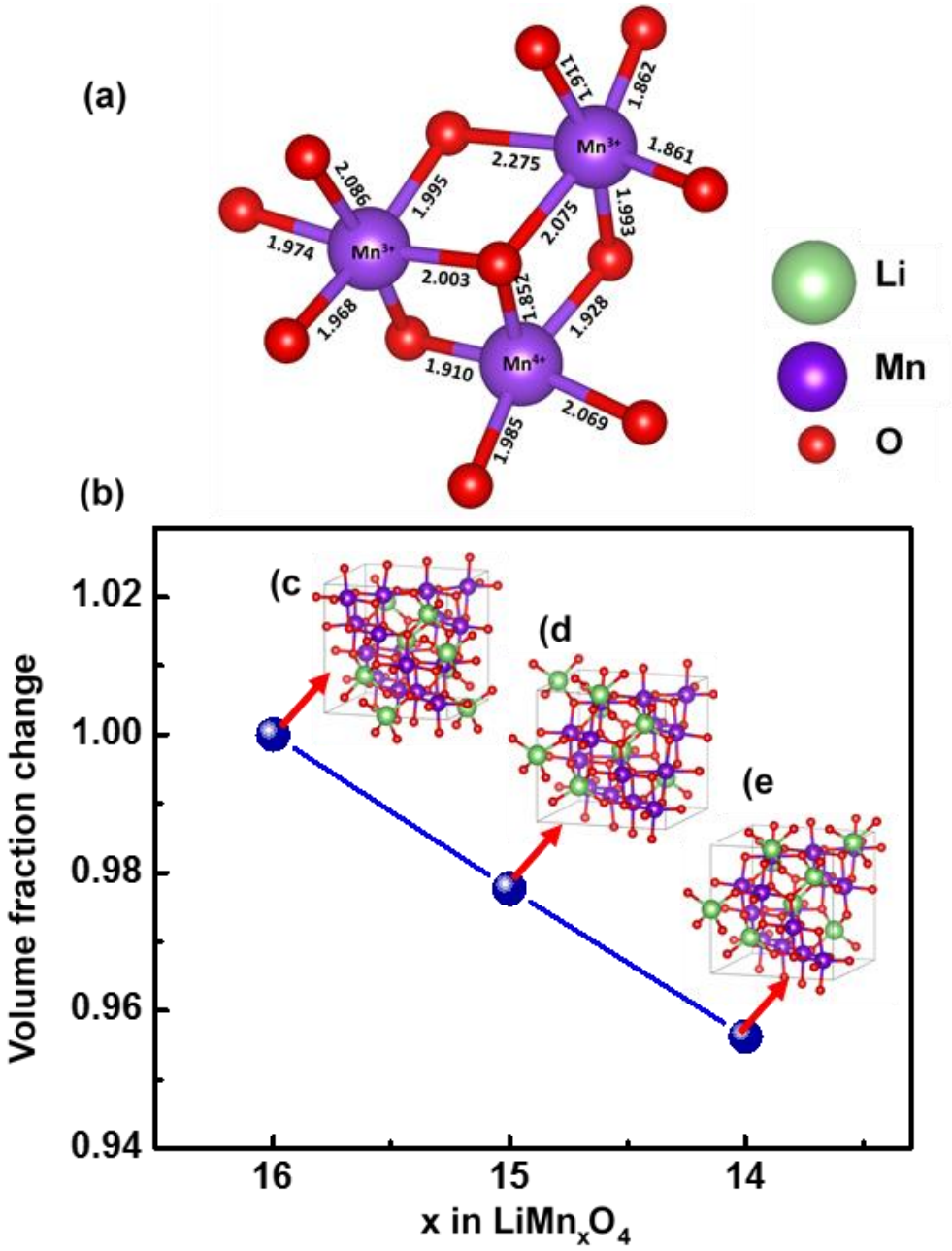

Figure 5. **(**a) Local atomic positions around Mn^{3+} and Mn^{4+} in $LiMn_2O_4$; (b) Active material volume fraction Change after removing Mn^{3+} from bulk 8 $LiMn_2O_4$; (c)–(e) shows the change in bulk structure after removing 1 Mn^{3+} after each step.

Dissolution of active materials affects battery performance in several ways. Transition metal ion dissolution aggravates the capacity fading by disintegrating the

electrode material into the electrolyte solution. Moreover, the deposition of electronically insulating side products on the cathode leads to a rise in internal impedance.[63],[64] At low State of Charge (SOC), the Mn oxidation status change from trivalent (3+) to tetravalent (4+) and divalent (2+) and, in this disproportion reaction, solvated Mn^{2+} causes the degradation of the cell. At higher SOC levels, the dissolution reaction is mainly governed by the hydrofluoric acid (HF) attack.[65] Also, at elevated temperatures, more manganese ions undergo dissolution from small $LiMn_2O_4$ particles than from large particles and cause a capacity loss due to structural disorder.[66] Crack propagation in coated and uncoated particle is coupled with dissolution physics. Mn dissolution during cycling is much more severe than the static condition. To include this cycling effect, a multiplication factor of 37.5 was used, as observed experimentally.[56] As the cycle number increases, the volume fraction of the active material decreased and the amount of dissolved manganese ions increased. The decrease in electrolyte volume fraction immediately resulted in a nonlinear decrease in effective Li-ion diffusion and conduction in the electrolyte. Consequently, a decrease in effective transport properties resulted in the poor performance of the Li-ion cell. The effective volume fraction of the active materials changed continuously due to the dissolution of manganese, specifically Mn^{3+} ions and, thus, the effective transport properties in the solid phase were changed with the cycling process. To evaluate the volume fraction change due to dissolution, the relationship between the dissolution mechanism and storage time was used. In the previous study, it was shown that the dissolution reaction was mostly controlled by the reaction at the unreacted core and can be expressed by[66]

$$[1-(1-Xa)^{\frac{1}{3}}] = kt \quad (10)$$

Where t is the reaction time, k is the reaction rate constant, and X_a is the conversion of the dissolution reaction. The reaction rates for the UC sample and 3nm-Ce sample were found to be 1.008×10^{-9} and 2.852×10^{-10} s^{-1}, respectively. The conversion of the dissolution reaction (X_a) is defined as

$$X_a = \frac{(dissolved\ Mn^{2+} mole\ in\ the\ electrolyte)\times 2}{Mn^{3+}\ mole\ in\ the\ electrolyte}$$

$$X_a = \frac{m_d \times 2}{(m_i - m_d)} \quad (11)$$

After determining the X_a initially (m_d =0), the reaction rate constant k was calculated from Eq. (11). The k values for the UC sample and the 3nm-Ce sample were 1.008×10^{-9} and 2.852×10^{-10} s^{-1}, respectively. Volume fraction change was calculated using the formula[67]

$$V(t) = V_i\left(1-\frac{0.304}{2}\frac{Xa}{Xa+1}\right) \quad (12)$$

To confirm the estimated value, a DFT calculation was made. To effectively see the effect of Mn^{3+} dissolution, the Mn^{3+} and Mn^{4+} ions in a $LiMn_2O_4$ system was identified initially. Shown in Figure 5(a) are the local atomic structures of $LiMn_2O_4$. The detailed bond lengths presented in Figure 5(a) show that the average Mn-O bond length of Mn^{4+} was smaller than that the average of Mn^{3+} ion. To see the volume fraction change, after removing Mn^{3+}, the total energy of the bulk system was calculated by removing Mn^{3+}one by one and then determining the Mn^{3+} corresponding to the lowest energy state. The Mn^{3+} with the lowest energy state was removed from the bulk structure and the corresponding volume change was calculated. After removing the 1st Mn^{3+}, the volume change was found to be 2.23%. Then, all of the remaining Mn^{3+} was removed, to find the lowest energy Mn^{3+},

and the volume change was recalculated. The volume change related to the smallest energy state was found to be 4.37%. Figure 5(b) shows the reduction in the volume fraction of active materials after removing the Mn^{3+} ions ($LiMn_{2-x}O_4$) from the original structure. The change in volume of the uncoated particle, after losing the manganese in static condition (shown in Figure 5(a)) was obtained from an analytical solution and DFT calculation. Although the volume fraction changes, based on the DFT, were slightly different from the analysis results, they were in a similar range. From the calculation, it could be confirmed that the uncoated particles showed higher volume changes, as there was no protective barrier between the electrode and electrolyte, which led to performance degradation.

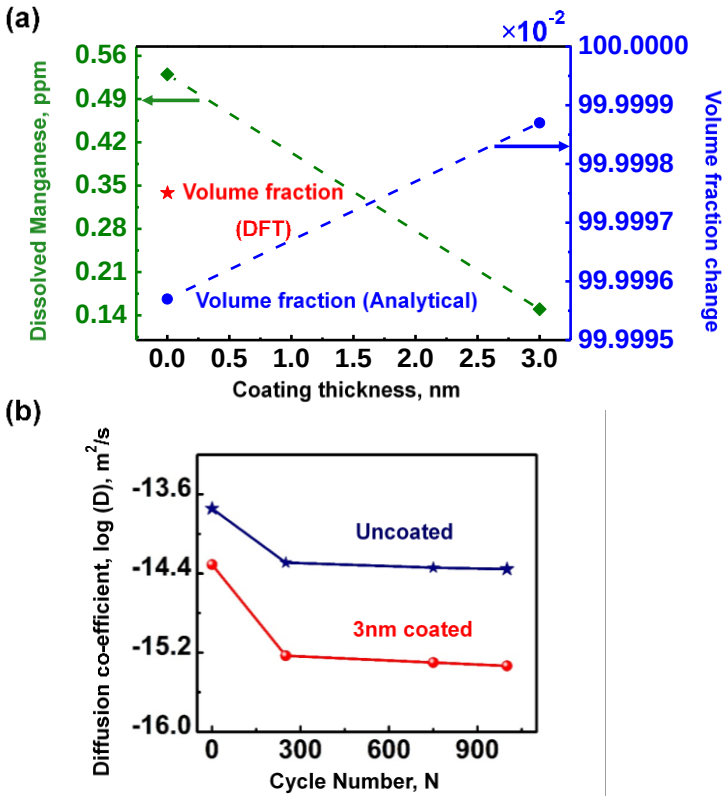

Figure 6. **(**a) Dissolve manganese and volume fraction change as a function of coating thickness. Volume change for UC particle was calculated both from analytical and DFT calculation; (b) Diffusion Co-efficient change for UC and 3nm-Ce particles as a function of cycle number.

To understand the effect of a coating layer on manganese dissolution, the amount of manganese dissolved from the cathode was measured using ICP-OES. The results are shown in Figure 6(a). The results demonstrated that the uncoated particles have accelerated the dissolution process. For example, after 5 weeks at room temperature, manganese in a bare electrode dissolved 3.5 times faster than that in a 3 nm coated electrode. The diffusion coefficients of the uncoated and 3nm-Ce particles were calculated as a function of the cycle number, as shown in Figure 6(b). The diffusion coefficient changed dramatically with increases in the cycle number. In the case of uncoated particles, larger amounts of dissolved manganese significantly increased the charge transfer resistance and contact resistance, which also delayed the Li-ion transportation.

Next, the all-inclusive mechano-electrochemical impact of ALD coating on a positive electrode was determined by fusing stress buildup, crack augmentation, ionic diffusivity, electronic conductivity, and transition metal-ion dissolution to evaluate the actual performance of the operating battery. Galvanostatic charge/discharge simulations, with voltage ranging between 4.4 V and 3.2 V, were executed. Figure 7 (a)-(d) shows representative discharge profiles. It can be noticed from the graph that all of the coated particles exhibited higher final capacities after 1,000 cycles than the uncoated particles did at either temperature. Among the coated particles, 3nm CeO_2 coating showed the highest capacity, which was in good agreement with experimental observations. The major concern with the bare positive electrode was the buildup of high-level stress on the surface due to the slower insertion/extraction of lithium ions, which consecutively generated crack growth. Additionally, it cannot provide shielding from dissolution. Given that the ALD-coated electrode is superior in chemical stability, it protects active materials by delaying

degradation in the regular condition and, also, by decelerating capacity fading during cycling. Of all coating thicknesses, the 3nm-Ce increased lithium diffusivity and electronic conductivity significantly by lowering the resistivity of the materials.

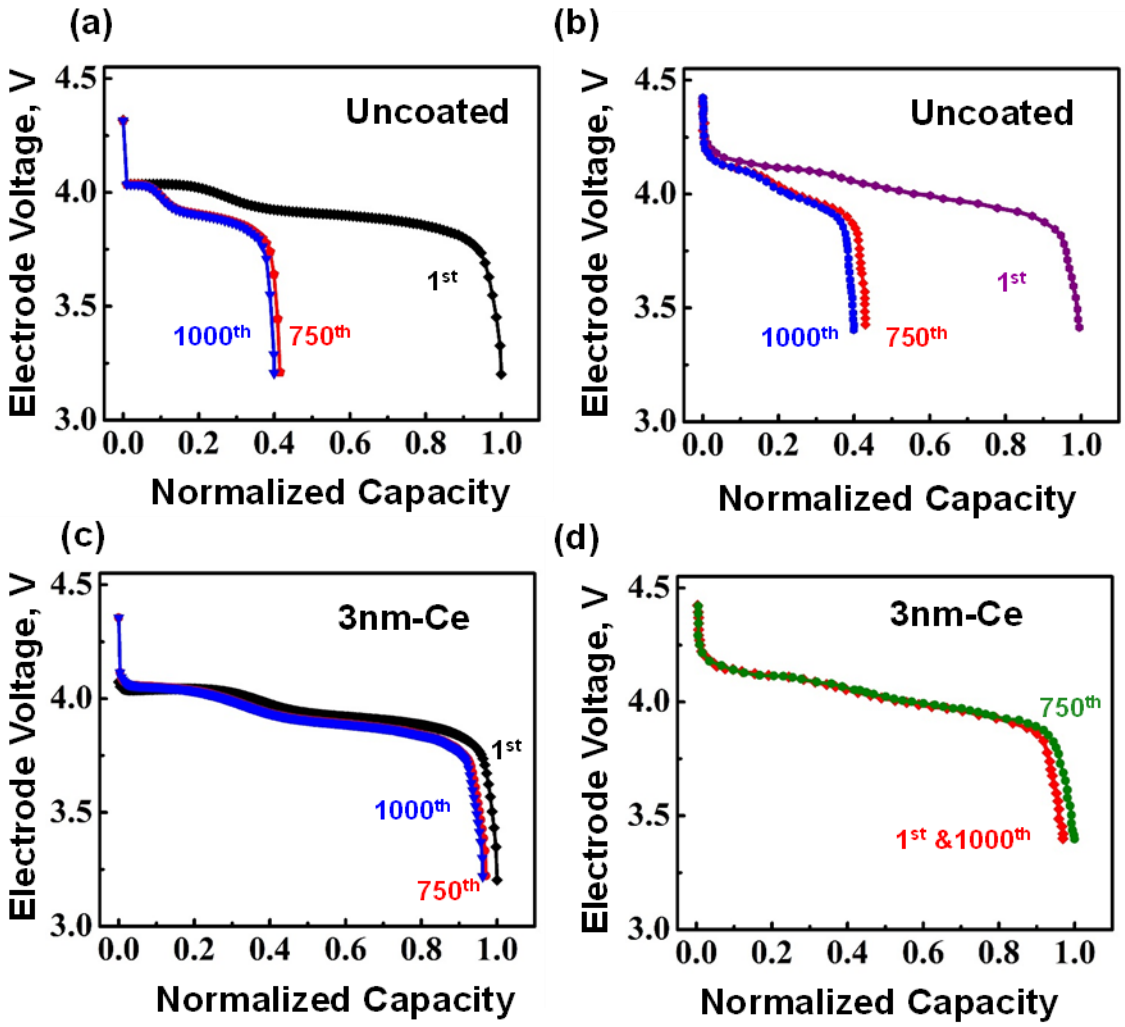

Figure 7. Discharge voltage profiles for uncoated particles (a) simulation and (b) experiment, and 3nm coated particles (c) simulation and (d) experiment. 3nm coated particles showed more significant cycle life improvement than the uncoated particles did.

It is worth noting that, although the 2 nm and 5 nm coatings had lower stress evolution and transition metal ion dissolution than the bare particles, the insignificant lithium ion diffusivity (comparable to that of the bare particles), it did not show much

improved battery performance. In uncoated LMO-based composite electrodes, stress induced crack, lower conductivity, and lower capacity utilization (due to the loss of active materials from acidic HF in the electrolyte) advanced fast capacity fading. Nonetheless, the results do advocate that optimal coating thickness can conquer the trade-off between ionic diffusivity, stress initiation, crack propagation, and shielding.

5. CONCLUSIONS

The proposed experiments and simulations revealed a correlation between the mechanical and electrochemical properties of positive electrodes made of CeO_2 ALD coated particles. On the mechanical side, it has been demonstrated that thin ALD coatings can only provide a limited mechanical protection to LMO particles. From an electrochemical point of view, the continuous increase in thickness of the CeO_2 coating does not facilitate the Li ion diffusivity and electronic conductivity. The balance between mechanical stability, transport delay, and side reaction prevention requires an optimal thickness of ALD coating to maximize the performance of LIBs. This report provides an interconnecting link between observed performance and improvement paths via ALD coatings.

ACKNOWLEDGEMENTS

The authors gratefully acknowledge financial support from the National Science Foundation (CBET 1510085) and the Missouri University Research Award (UMRB FEB2015).

REFERENCES

[1] Z. Chen, Y. Qin, K. Amine, Role of surface coating on cathode materials for lithium-ion batteries, J. Mater. Chem. 20 (2010) 7606–7612. doi:10.1039/c0jm00154f.

[2] B.L. Cushing, J.B. Goodenough, Influence of carbon coating on the performance of a LiMn0.5Ni0.5O2 cathode, Solid State Sci. 4 (2002) 1487–1493. doi:10.1016/S1293-2558(02)00044-4.

[3] J.S. Park, X. Meng, J.W. Elam, C. Wolverton, C. Kim, J. Cabana, Ultrathin Lithium Ion Conducting Coatings for Increased Interfacial Stability in High Voltage Li-ion Batteries Ultrathin Lithium Ion Conducting Coatings for Increased Interfacial Stability in High Voltage Li-ion Batteries, Chem. Mater. 26 (2014) 3128–3134. doi:10.1021/cm500512n.

[4] J. Liu, L. Yu, C. Wu, Y. Wen, K. Yin, F.K. Chiang, R. Hu, J. Liu, L. Sun, L. Gu, J. Maier, Y. Yu, M. Zhu, New Nanoconfined Galvanic Replacement Synthesis of Hollow Sb@C Yolk-Shell Spheres Constituting a Stable Anode for High-Rate Li/Na-Ion Batteries, Nano Lett. 17 (2017) 2034–2042. doi:10.1021/acs.nanolett.7b00083.

[5] L. Yu, J. Liu, X. Xu, L. Zhang, R. Hu, J. Liu, L. Yang, M. Zhu, Metal-organic framework-derived NiSb alloy embedded in carbon hollow spheres as superior lithium-ion battery anodes, ACS Appl. Mater. Interfaces. 9 (2017) 2516–2525. doi:10.1021/acsami.6b14233.

[6] J. Liu, X. Xu, R. Hu, L. Yang, M. Zhu, Uniform Hierarchical Fe3O4@Polypyrrole Nanocages for Superior Lithium Ion Battery Anodes, Adv. Energy Mater. 6 (2016) 1–7. doi:10.1002/aenm.201600256.

[7] Y.J. Kim, J. Cho, T.-J. Kim, B. Park, Suppression of Cobalt Dissolution from the LiCoO[sub 2] Cathodes with Various Metal-Oxide Coatings, J. Electrochem. Soc. 150 (2003) A1723. doi:10.1149/1.1627347.

[8] J. Cho, Y.J. Kim, Enhanced Structural Stability of o-LiMnO2 by Sol-Gel Coating of Al2O3, Chem. Mater. 13 (2001) 18–20.

[9] M. Zhang, N. Garcia-Araez, A.L. Hector, J.R. Owen, A sol–gel route to titanium nitride conductive coatings on battery materials and performance of TiN-coated $LiFePO_4$, J. Mater. Chem. A. 5 (2017) 2251–2260. doi:10.1039/C6TA09572K.

[10] H.M. Omanda, R.O. Ndong, A.E.Y.A. A-mvongbote, Z.H.M. Membetsi, Modifying of LiNi 0 . 8 Co 0 . 2 O 2 Cathode Material by Chemical Vapor Deposition Coating to Improve Thermal Stability, 3 (2013) 59–67.

[11] R. Tian, H. Liu, Y. Jiang, J. Chen, X. Tan, G. Liu, L. Zhang, X. Gu, Y. Guo, H. Wang, L. Sun, W. Chu, Drastically Enhanced High-Rate Performance of Carbon-Coated LiFePO 4 Nanorods Using a Green Chemical Vapor Deposition (CVD) Method for Lithium Ion Battery: A Selective Carbon Coating Process, ACS Appl. Mater. Interfaces. 7 (2015) 11377–11386. doi:10.1021/acsami.5b01891.

[12] X. Li, J. Liu, M.N. Banis, A. Lushington, R. Li, M. Cai, X. Sun, Atomic layer deposition of solid-state electrolyte coated cathode materials with superior high-voltage cycling behavior for lithium ion battery application, Energy Environ. Sci. 7 (2014) 768. doi:10.1039/c3ee42704h.

[13] K. Gregorczyk, M. Knez, Hybrid nanomaterials through molecular and atomic layer deposition: Top down, bottom up, and in-between approaches to new materials, Prog. Mater. Sci. 75 (2016) 1–37. doi:10.1016/j.pmatsci.2015.06.004.

[14] V. Miikkulainen, M. Leskela, M. Ritala, R.L.P. Puurunen, Crystallinity of inorganic films grown by atomic layer deposition: Overview and general trends, 2013. doi:10.1063/1.4757907.

[15] S.M. George, A.W. Ott, J.W. Klaus, Surface chemistry for atomic layer growth, J. Phys. Chem. 100 (1996) 13121–13131. doi:DOI 10.1021/jp9536763.

[16] S. George, Atomic layer Deposition: An Overview, Chem. Rev. 110 (2010) 111–131. doi:10.1021/cr900056b.

[17] F. Zaera, The surface chemistry of atomic layer depositions of solid thin films, J. Phys. Chem. Lett. 3 (2012) 1301–1309. doi:10.1021/jz300125f.

[18] J. Zheng, M. Gu, J. Xiao, B.J. Polzin, P. Yan, X. Chen, C. Wang, J.G. Zhang, Functioning mechanism of AlF3 coating on the Li- and Mn-rich cathode materials, Chem. Mater. 26 (2014) 6320–6327. doi:10.1021/cm502071h.

[19] M.-S. Wang, J. Wang, J. Zhang, L.-Z. Fan, Improving electrochemical performance of spherical LiMn2O4 cathode materials for lithium ion batteries by Al-F codoping and AlF3 surface coating, Ionics (Kiel). 21 (2014) 27–35. doi:10.1007/s11581-014-1164-6.

[20] Y.-K. Sun, S.-W. Cho, S.-W. Lee, C.S. Yoon, K. Amine, AlF3-Coating to Improve High Voltage Cycling Performance of Li[Ni1⁄3Co1⁄3Mn1⁄3]O2 Cathode Materials for Lithium Secondary Batteries, J. Electrochem. Soc. 154 (2007) A168. doi:10.1149/1.2422890.

[21] W. Li, X. Li, M. Chen, Z. Xie, J. Zhang, S. Dong, M. Qu, AlF3 modification to suppress the gas generation of Li 4Ti5O12 anode battery, Electrochim. Acta. 139 (2014) 104–110. doi:10.1016/j.electacta.2014.07.017.

[22] Y.S. Jung, A.S. Cavanagh, L.A. Riley, S.H. Kang, A.C. Dillon, M.D. Groner, S.M. George, S.H. Lee, Ultrathin direct atomic layer deposition on composite electrodes for highly durable and safe Li-Ion batteries, Adv. Mater. 22 (2010) 2172–2176. doi:10.1002/adma.200903951.

[23] X. Xiao, P. Lu, D. Ahn, Ultrathin multifunctional oxide coatings for lithium ion batteries, Adv. Mater. 23 (2011) 3911–3915. doi:10.1002/adma.201101915.

[24] J. Zhai, M. Zhao, D. Wang, Y. Qiao, Effect of MgO nanolayer coated on Li3V2(PO4)3/C cathode material for lithium-ion battery, J. Alloys Compd. 502 (2010) 401–406. doi:10.1016/j.jallcom.2010.04.181.

[25] Y.-D. Li, S.-X. Zhao, C.-W. Nan, B.-H. Li, Electrochemical performance of SiO2-coated LiFePO4 cathode materials for lithium ion battery, J. Alloys Compd. 509 (2011) 957–960. doi:10.1016/j.jallcom.2010.08.154.

[26] Y. Cho, J. Cho, Significant Improvement of LiNi0.8Co0.15Al0.05O2 Cathodes at 60°C by SiO2 Dry Coating for Li-Ion Batteries, J. Electrochem. Soc. 157 (2010) A625. doi:10.1149/1.3363852.

[27] Z. Chen, J.R. Dahn, Effect of a ZrO[sub 2] Coating on the Structure and Electrochemistry of Li[sub x]CoO[sub 2] When Cycled to 4.5 V, Electrochem. Solid-State Lett. 5 (2002) A213. doi:10.1149/1.1503202.

[28] J. Zhao, G. Qu, J.C. Flake, Y. Wang, Low temperature preparation of crystalline ZrO2 coatings for improved elevated-temperature performances of Li-ion battery cathodes, Chem. Commun. 48 (2012) 8108. doi:10.1039/c2cc33522k.

[29] X. Zhang, I. Belharouak, L. Li, Y. Lei, J.W. Elam, A. Nie, X. Chen, R.S. Yassar, R.L. Axelbaum, Structural and Electrochemical Study of Al2O3 and TiO2 Coated Li1.2Ni0.13 Mn0.54Co0.13O2 Cathode Material Using ALD, Adv. Energy Mater. 3 (2013) 1299–1307. doi:10.1002/aenm.201300269.

[30] R.L. Patel, H. Xie, J. Park, H.Y. Asl, A. Choudhury, X. Liang, Significant Capacity and Cycle-Life Improvement of Lithium-Ion Batteries through Ultrathin Conductive Film Stabilized Cathode Particles, Adv. Mater. Interfaces. 2 (2015). doi:10.1002/admi.201500046.

[31] M. Gaberscek, R. Dominko, J. Jamnik, Is small particle size more important than carbon coating? An example study on LiFePO4 cathodes, Electrochem. Commun. 9 (2007) 2778–2783. doi:10.1016/j.elecom.2007.09.020.

[32] A.R. Armstrong, M. Holzapfel, S.H. Kang, P. Nova, S. Kang, M.M. Thackeray, P.G. Bruce, Demonstrating Oxygen Loss and Associated Structural Reorganization in the Lithium Battery Cathode Li[Ni0.2Li0.2Mn0.6]O2, J. Am. Chem. Soc. 128 (2006) 8694–8698. doi:10.1021/ja062027.

[33] M. Aykol, S. Kirklin, C. Wolverton, Thermodynamic aspects of cathode coatings for lithium-ion batteries, Adv. Energy Mater. 4 (2014) 1–11. doi:10.1002/aenm.201400690.

[34] H. Li, H. Zhou, Enhancing the performances of Li-ion batteries by carbon-coating: present and future, Chem. Commun. 48 (2012) 1201. doi:10.1039/c1cc14764a.

[35] Y.-K. Sun, Y.-S. Lee, M. Yoshio, K. Amine, Synthesis and Electrochemical Properties of ZnO-Coated LiNi0.5Mn1.5O4 Spinel as 5 V Cathode Material for Lithium Secondary Batteries, Electrochem. Solid-State Lett. 5 (2002) A99. doi:10.1149/1.1465375.

[36] W.M. Zhang, J.S. Hu, Y.G. Guo, S.F. Zheng, L.S. Zhong, W.G. Song, L.J. Wan, Tin-nanoparticles encapsulated in elastic hollow carbon spheres for high-performance anode material in lithium-ion batteries, Adv. Mater. 20 (2008) 1160–1165. doi:10.1002/adma.200701364.

[37] S.C. Jung, Y.-K. Han, How Do Li Atoms Pass through the Al 2 O 3 Coating Layer during Lithiation in Li-ion Batteries?, J. Phys. Chem. Lett. (2013) 2681–2685. doi:10.1021/jz401231e.

[38] S. Xu, R.M. Jacobs, H.M. Nguyen, S. Hao, M. Mahanthappa, C. Wolverton, D. Morgan, Lithium transport through lithium-ion battery cathode coatings, J. Mater. Chem. A. 3 (2015) 17248–17272. doi:10.1039/C5TA01664A.

[39] K. Leung, Y. Qi, K.R. Zavadil, Y.S. Jung, A.C. Dillon, A.S. Cavanagh, S.-H. Lee, S.M. George, Using atomic layer deposition to hinder solvent decomposition in lithium ion batteries: first principles modeling and experimental studies., J. Am. Chem. Soc. (2011) 14741–14754. doi:10.1021/ja205119g.

[40] R.L. Patel, J. Park, X. Liang, Ionic and electronic conductivities of atomic layer deposition thin film coated lithium ion battery cathode particles, RSC Adv. 6 (2016) 98768–98776. doi:10.1039/C6RA20829K.

[41] J. Park, S. Kalnaus, S. Han, Y.K. Lee, G.B. Less, N.J. Dudney, C. Daniel, A.M. Sastry, In situ atomic force microscopy studies on lithium (de)intercalation-induced morphology changes in LixCoO2 micro-machined thin film electrodes, J. Power Sources. 222 (2013) 417–425. doi:10.1016/j.jpowsour.2012.09.017.

[42] A.H. Wiedemann, G.M. Goldin, S.A. Barnett, H. Zhu, R.J. Kee, Effects of three-dimensional cathode microstructure on the performance of lithium-ion battery cathodes, Electrochim. Acta. 88 (2013) 580–588. doi:10.1016/j.electacta.2012.10.104.

[43] Y.K. Lee, Effects of Tansition Metal Dissolution and Deposition on Li-ion Batteries : A Multi-scale approach, (2015).

[44] A.A. Williams, J. Park, S. Byun, M. Ryou, Y.M. Lee, A Mathematical Model for Cyclic Aging of Spinel LiMn2O4/Graphite Lithium-Ion Cells, J. Electrochem. Soc. 163 (2016) A2757–A2767. doi:10.1149/2.1061613jes.

[45] J.P. Perdew, K. Burke, M. Ernzerhof, Generalized Gradient Approximation Made Simple, Phys. Rev. Lett. 77 (1996) 3865–3868. doi:10.1103/PhysRevLett.77.3865.

[46] G. Kresse, From ultrasoft pseudopotentials to the projector augmented-wave method, Phys. Rev. B. 59 (1999) 1758–1775. doi:10.1103/PhysRevB.59.1758.

[47] G. Kresse, J. Hafner, Ab initio molecular dynamics for liquid metals, Phys. Rev. B. 47 (1993) 558–561. doi:10.1103/PhysRevB.47.558.

[48] M. Park, X. Zhang, M. Chung, G.B. Less, A.M. Sastry, A review of conduction phenomena in Li-ion batteries, J. Power Sources. 195 (2010) 7904–7929. doi:10.1016/j.jpowsour.2010.06.060.

[49] C.-Y. Kim, S.-G. Cho, T.-Y. Lim, D.-K. Choi, Anomalous lithium ion diffusion into CeO 2 ·TiO 2 thin film by film thickness variations, J Solid State Electrochem. 13 (2009) 1165–1170. doi:10.1007/s10008-008-0633-0.

[50] S. Mandal, J.M. Amarilla, J. Ibáñez, J.M. Rojo, The Role of Carbon Black in LiMn 2 O 4 -Based Composites as Cathodes for Rechargeable Lithium Batteries, (2001).

[51] X. Han, Y. Liu, Z. Jia, Y.-C. Chen, J. Wan, N. Weadock, K.J. Gaskell, T. Li, L. Hu, Atomic-Layer-Deposition Oxide Nanoglue for SodiumIon Batteries., Nano Lett. 14 (2014) 139–147. doi:10.1021/nl4035626.

[52] M. Zhu, J. Park, A.M. Sastry, Fracture Analysis of the Cathode in Li-Ion Batteries: A Simulation Study, J. Electrochem. Soc. 159 (2012) A492. doi:10.1149/2.045204jes.

[53] C.-K. ChiuHuang, H.-Y. Shadow Huang, Stress Evolution on the Phase Boundary in LiFePO4 Particles, J. Electrochem. Soc. 160 (2013) A2184–A2188. doi:10.1149/2.079311jes.

[54] M. A. Stamps, J. W. Eischen, H.-Y. Shadow Huang, Particle- and crack-size dependency of lithium-ion battery materials $LiFePO_4$, AIMS Mater. Sci. 3 (2016) 190–203. doi:10.3934/matersci.2016.1.190.

[55] J. Park, W. Lu, A.M. Sastry, Numerical Simulation of Stress Evolution in Lithium Manganese Dioxide Particles due to Coupled Phase Transition and Intercalation, J. Electrochem. Soc. 158 (2011) A201. doi:10.1149/1.3526597.

[56] Y. Xia, Capacity Fading on Cycling of 4 V Li/LiMn2O4Cells, J. Electrochem. Soc. 144 (1997) 2593. doi:10.1149/1.1837870.

[57] H. Shaikh, T. Anita, A. Poonguzhali, R.K. Dayal, B. Raj, Stress Corrosion Cracking, 2011. doi:10.1533/9780857093769.3.427.

[58] U. Hejman, C. Bjerken, Dissolution driven crack branching in polycarbonate, Fatigue Fract. Eng. Mater. Struct. 34 (2011) 227–239. doi:10.1111/j.1460-2695.2010.01508.x.

[59] C. Bjerkén, Branching of a dissolution driven stress corrosion crack, (n.d.) 1073–1080.

[60] K. Edström, T. Gustafsson, J.O. Thomas, The cathode-electrolyte interface in the Li-ion battery, in: Electrochim. Acta, 2004: pp. 397–403. doi:10.1016/j.electacta.2004.03.049.

[61] D. Aurbach, B. Markovsky, G. Salitra, E. Markevich, Y. Talyossef, M. Koltypin, L. Nazar, B. Ellis, D. Kovacheva, Review on electrode-electrolyte solution interactions, related to cathode materials for Li-ion batteries, J. Power Sources. 165 (2007) 491–499. doi:10.1016/j.jpowsour.2006.10.025.

[62] W. Liu, J. Liu, K. Chen, S. Ji, Y. Wan, Y. Zhou, D. Xue, P. Hodgson, Y. Li, Enhancing the electrochemical performance of the LiMn2O 4 hollow microsphere cathode with a LiNi0.5Mn 1.5O4 coated layer, Chem. - A Eur. J. 20 (2014) 824–830. doi:10.1002/chem.201303675.

[63] J.M. Tarascon, M. Armand, Issues and challenges facing rechargeable lithium batteries., Nature. 414 (2001) 359–67. doi:10.1038/35104644.

[64] C. Lin, A. Tang, H. Mu, W. Wang, C. Wang, Aging Mechanisms of Electrode Materials in Lithium-Ion Batteries for Electric Vehicles, 2015 (2015) 1–18. doi:10.1155/2015/104673.

[65] J. Vetter, P. Novák, M.R. Wagner, C. Veit, K.C. Möller, J.O. Besenhard, M. Winter, M. Wohlfahrt-Mehrens, C. Vogler, A. Hammouche, Ageing mechanisms in lithium-ion batteries, J. Power Sources. 147 (2005) 269–281. doi:10.1016/j.jpowsour.2005.01.006.

[66] C.-H. Lu, S.-W. Lin, Dissolution Kinetics of Spinel Lithium Manganate and its Relation to Capacity Fading in Lithium Ion Batteries, J. Mater. Res. 17 (2002) 1476–1481. doi:10.1557/JMR.2002.0219.

[67] J. Park, J.H. Seo, G. Plett, W. Lu, A.M. Sastry, Numerical Simulation of the Effect of the Dissolution of LiMn2O4 Particles on Li-Ion Battery Performance, Electrochem. Solid-State Lett. 14 (2011) A14. doi:10.1149/1.3516619.

II. MICRO-MACROSCOPIC MODELING OF A LITHIUM-ION CELL BY CONSIDERING GRAIN BOUNDARIES OF ACTIVE MATERIALS

Susmita Sarkar[1], John Hoffmann[1], Jonghyun Park[1,*]

[1]Department of Mechanical Engineering, Missouri University of Science and Technology, Rolla, MO 65409, United States

*Corresponding author Email: parkjonghy@mst.edu

ABSTRACT

Many important properties of electrode materials are profoundly sensitive to deviations from the crystalline perfection. Among them are grain boundaries that play an important role on battery performance by changing the ions distribution inside particles and corresponding stress level change. This paper explores the mechanical and microstructural aspect of battery behavior by developing a cell-level model that incorporates grain boundary diffusion in the electrode particles for the anode and cathode electrodes. The developed model is compared against the grainless model at various operating conditions to understand how grain boundaries influence capacity and stress generation. The results show an appreciable effect of grain boundary diffusion on the voltage profile for the cell for the parameters tested and, overall, a significant reduction in the maximum induced stress experienced in the cell. Stress behavior between the anode and cathode differ significantly, and show that the effective diffusivity of a particle might matter much more significantly than its location in the cell.

1. INTRODUCTION

As concern over climate change rises and the ecological effects of petroleum production are debated, the need to replace or supplement traditional internal combustion energy vehicles with commercial vehicles using alternative fuel sources has become apparent. The leading candidate, by way of fuel efficiency and ease of infrastructure construction, in this category is the electric vehicle. But this decade has seen the entry of several leading automotive manufacturers into the electric vehicle market with cars that were priced more affordably and designed to compete with their internal combustion counterparts. The technology to enable this new wave of vehicles is the lithium ion battery.

The lithium ion battery is suitable for this because it has a high capacity, meaning the total charge able to be stored, and can provide high power output for those applications that need it. Most of the host materials in Li-ion batteries are transition metal oxides with stable crystal lattices providing the pathways for Li-ions to diffuse. Also, most of the material modeling in the battery field has been tacitly assumed that perfect order exists throughout crystalline materials. However, all crystalline materials for the active materials in Li-ion batteries contain large number of various defects or imperfections. Many important properties of the electrode materials are profoundly sensitive to deviations from the crystalline perfection such as point, interfacial, and bulk defects. Among them, grain boundary, which belongs to interfacial defect, plays an important role on the battery performance in several ways.

The diffusivity within the grain boundaries is much higher than in the crystal due to the low activation energy for diffusion caused by loosely packed structures in the

boundaries. For instance, nanoscale polycrystalline materials, the measured activation energy for self-diffusion at the grain boundaries is only a fraction of that in the grain, resulting in 3-16 orders of magnitude higher diffusivity in the grain boundary than in the grain [1–3]. These experiments show that as the average grain size is refined to nanoscale, the grain boundary dominates the transport properties. In addition, due to higher diffusivity within the grain boundary than the grain, the Li-ion penetrates much deeper along the grain boundary. This affects the Li-ion concentration distribution inside the particle leading to stress state change in an active material particle. The intercalation-induced stress is estimated one of the key degradation mechanisms in Li-ion batteries because it can cause structural instability leading to material isolation and increase of side reaction.

The effects of the grain boundary, especially focused on diffusivity, in the active materials for Li-ion battery applications have been studies in several works. High density of grain boundaries in nanocomposites provides a fast diffusion path for lithium ions. Besides the grain boundary density, several reports have suggested that grain orientations may have a more significant impact on the overall lithium ion diffusivity, especially for materials with two dimensional diffusion mechanisms such as $LiCoO_2$ [4] and V_2O_5 [5]. Also, some modeling efforts have been conducted to understand the effects of the grain boundary on diffusivity. Assuming that the concentration of diffusing species is constant across the thin grain boundary, Fisher modeled a single fast diffusing grain boundary embedded in a semi-infinite bulk of much lower diffusivity [6]. The model and its variants are widely used today in understanding the grain boundary diffusion. Additional studies have been carried out to calculate the effective diffusion coefficient based on diffusivities

in grains and grain boundaries, average grain size, grain boundary thickness, and grain boundary network geometry [7–11].

The act of lithium ions entering and leaving the electrode material is respectively known as intercalation and de-intercalation, and is associated with a localized volume swelling in the bulk material similar to an object undergoing heating and cooling. While the system eventually experiences little stress as the ion concentration diffuses and expansion becomes uniform, in the transient periods of charge and discharge, uneven lithium concentration can lead to high induced stresses. These Eigen stresses, stresses generated internally via inhomogeneity instead of external loading, can be so pronounced that silicon, though possessing a specific energy density tenfold that of graphite, is unusable due to a 400% volume expansion that causes significant cracking and material loss that significantly diminish the possible lifespan achievable [12]. Capturing the physical stress-strain effect, while not new, does mark a deviation from the traditional electro-chemical model.

While the effect of grain boundaries in Li-ion battery has been postulated based on experimental results, their specific role has not been studied systematically. This is possibly due to the difficulty in synthesizing active materials with different grain boundary densities but identical material phase and grain orientation distributions. The effect of grain boundary on battery performance may be quantified through modeling and simulations. The focus of this investigation is the incorporation of the effects of grain boundaries on cell performance and stress generation. Electrode particles are small enough that assumptions of homogeneity and ideal shape that are adequate on the macroscale are likely unsuitable. Particles are marked by highly heterogeneous microstructural features. Grain

boundaries are the small regions separating the grains, the monocrystalline elements of a polycrystalline material. Diffusivity of Lithium Ions inside the grain boundary can be much higher than in the grain, functioning as highways between the interior and exterior of the electrode. By increasing the effective diffusivity, it is thought that stresses generated in the electrode can be reduced and the total capacity can be increased. But since these grain boundaries are highly variant, it is necessary to test multiple variations.

The effects of grain boundary diffusion on capacity and stress generation have been explored on individual particles, with capacity utilization measured as the amount of Lithium particles intercalated over the amount the particle can theoretically hold [13]. Currently, this behavior has not been extended to the cell scale: how multiple particles with different, diffusive grain boundaries interact with each other when placed in the same electrode, and how they collectively affect the capacity of the cell in the traditional sense of time taken from upper cut-off voltage to lower cut-off voltage at a given current. Stress generation, on the cell scale, in P2D models have been explored, and have shown that single particle models do not adequately describe the stress variance across the electrode, but do not take grain structure into account [14]. This work is simply the extension of continuum grain boundary modeling into the cell scale.

2. METHODS

The traditional electrochemical model is the P2D (pseudo two dimensional) model. The P2D model describes, spatially, the three-dimensional real system by breaking it into two one-dimensional models: a cell scale model and a microscale model. Since the model

described in this paper also uses the cell-scale model, it will be described later. The microscale model represents a spherical, homogenous particle of active material. Flux around the surface of the particle is treated as constant. Due to the apparent symmetry of this problem, both angular dimensions of the sphere can be discounted and ion concentration only varies along the radial dimension.

The cell scale model describes the macroscale makeup of the model. A domain representing the entire internal length of the battery is trisected into three separate domains: the anode, the separator, and the cathode. Treating the height and width dimensions as infinite compared to the length, the properties (electrode and electrolyte electric potential) are treated solely as functions of the length dimension. It is important to note that, while the cathode and anode properties and differential equations are defined only on the right and left domain, the equations governing the electrolyte are defined on all three domains. This is because both electrodes are treated as porous and allow for electrolyte penetration. Equations (1) and (2) describe conservation of charge and mass diffusion in the electrolyte. The variable c_e represents ion concentration in the electrolyte and the variable φ_e represents potential in the electrolyte.

$$\nabla \cdot \left(\kappa_e^{eff} \left(\nabla \varphi_e - \frac{2RT}{F}(1 - t_+^0) \left(1 + \frac{d \ln f_{\pm}}{d \ln c_e} \right) \nabla \ln c_e \right) \right) + J^{Li} = 0 \tag{1}$$

$$\frac{\partial (\varepsilon_e c_e)}{\partial t} = \nabla \cdot \left(D_e^{eff} \nabla c_e \right) + \frac{1 - t_+^0}{F} J^{Li} - \frac{\mathbf{i_e} \cdot \nabla t_+^0}{F} \tag{2}$$

In the P2D model, the cell scale model is coupled to particle model such that the value of concentration at any time is defined by the cell scale lengthwise dimension (x) and the particle scale radial (r) dimension. This can be abstractly represented by a rectangle with its base aligned along the x axis and its height with the r axis. Ion diffusion primarily

happens along the radial dimension, and the coefficient of diffusion is dependent on the value of r due to the spherical nature of the particle. The top of the rectangle (where r is equal to the radius of the nanoparticle) is where flux between the electrode and electrolyte occurs by the Butler-Volmer equation (3). The quantity E-Eeq is sometimes known as the over-potential, denoted by η.

$$j = j_0 \cdot \left\{ \exp\left[\frac{\alpha_a z F}{RT}\left(E - E_{eq}\right)\right] - \exp\left[\frac{\alpha_c z F}{RT}\left(E - E_{eq}\right)\right] \right\} \tag{3}$$

In the new model used in this study, the assumption of a continuum of perfect, featureless spheres is dropped in favor of a discrete set of particles. The 1D cell scale model cathode portion is instead linked to an array of 3D quarter spheres. These quarter spheres represent a full particle by applying a zero flux condition through all non-curved surfaces. The Butler-Volmer equation controls flux, separate and invariant for each quarter sphere, through their curved surfaces. Conservation of charge (4) and Fick diffusion (5) equations control the movement of charge and ions in the grain boundary. The variable c_s represents ion concentration in the electrode and the variable φ_s represents potential in the electrode.

$$\nabla \cdot \left(\sigma_s^{eff} \nabla \varphi_s\right) - J^{Li} = 0 \tag{4}$$

$$\frac{\partial c_g}{\partial t} + \nabla \cdot \left[-D_g \left(\nabla c_g - \frac{\Omega c_g}{RT} \nabla \sigma_h\right)\right] = 0 \tag{5}$$

Five quarter spheres, representing particles equally spaced apart on the electrode, are used in this test. The lithium concentration is integrated over the curved surface and then divided out by the curved surface area to get the average surface concentration at that point in the electrode. With the five average concentrations, a fourth order polynomial

regression was used to generate a surface concentration profile over the whole macroscale electrode region.

If the new model was only what was just described, it could easily be converted from three dimensions to only one dimension due to symmetry. The model, however, also contains a three dimensional structure consisting of several two-dimensional planes, Voronoi partitions that represent the grain boundaries present in the particle. These grain boundaries are mathematically modeled through the Fisher model. The Fisher model, applicable when diffusion along the grain boundary is higher than the bulk material, assumes that ion concentration across the (relatively small) thickness of the grain boundary is constant and continuous. The grain boundary has its own diffusion coefficient and equation that allows ion passage along its tangential to itself. The ion conservation equation in a thin slab is described by the equation [6], where Jgb is the flux described by equation [7], where n is the direction normal to the slab and t1 and t2 are the tangential components of the slab.

$$\frac{\partial c_{gb}}{\partial t} + \nabla \cdot J_{gb} = 0 \tag{6}$$

$$J_{gb} = -D_{gb} \nabla c_{gb}(n, t_1, t_2, t) \tag{7}$$

By exploiting the assumptions made on the normal direction by the Fisher model, the 3-dimensional problem can be turned into a 2-dimensional problem solved over the Voronoi partitions. The resulting weak-form equations for the surfaces are given by equation [8].

$$n \cdot J_g|_{n=\pm\frac{\delta}{2}} = \mp\frac{\delta}{2}\int_S w\frac{\partial c_{gb}}{\partial t}\,dS \mp \frac{\delta}{2}\int_S D_{gb}\nabla_t w \cdot \nabla_t\, c_{gb}\,dS \tag{8}$$

The two-dimensional grain boundary equation is constrained to the three-dimensional bulk equation by having the concentration in the boundary equal to the concentration in the bulk. The expected result is that the grain boundaries have a lower resistance path in and out of the particle, affecting the maximum stresses induced in the particle and the behavior of the battery.

3. RESULTS

3.1. VALIDATION OF THE PROPOSED MODEL

First of all, the validation of the proposed approach, point-junction hierarchical approach, should be conducted. For this goal, the key variables in the cell-level model including the voltage response of a cell, Li-ion concentration in the solid phase and the liquid phase from the point-junction hierarchical approach are compared with results from one dimensional pseudo-2D model. The target cell is composed of the positive electrode, the separator, and the anode. The cell has following dimensions: negative electrode width is 100 um, separator is 52 um, and the positive electrode width is 183 um. The same material properties are used in both two models. In the point-junction hierarchical approach, uniformly distributed five spheres are located in the cathode domain. This number is quite enough to represent the cathode behavior because the relative thickness of the whole cathode electrode to the particle size is about 11.4. Considering volume fraction of active material and other additive material, there might be 5~8 particles through the thickness. This implies that the five particles can fully represent the cathode behavior. Each particle has isotropic material properties and has no grain boundary for this comparison. For the anode part, the conventional pseudo-2D model was adopted.

Figure 1 shows the discharge curve with different C rates. The cell was initially fully charged and was relaxed for 1000 seconds. Then, the cell was discharged with various current densities. The simulation was stopped when the cell voltage dropped down to 3.01 V. The nominal discharge current density of the cell is 17.5 A/m2 and the figure shows that this capacity can be obtained at around 1C. However, as the current density increases the capacity decreases due to high voltage drop coming from high polarization. As can be seen in the figure 1, the results from the both model are matched with each other at different c-rate (0.5C, 1C and 2C rate). Even at higher c-rate, there is not much deviation of proposed PJH from P2D model.

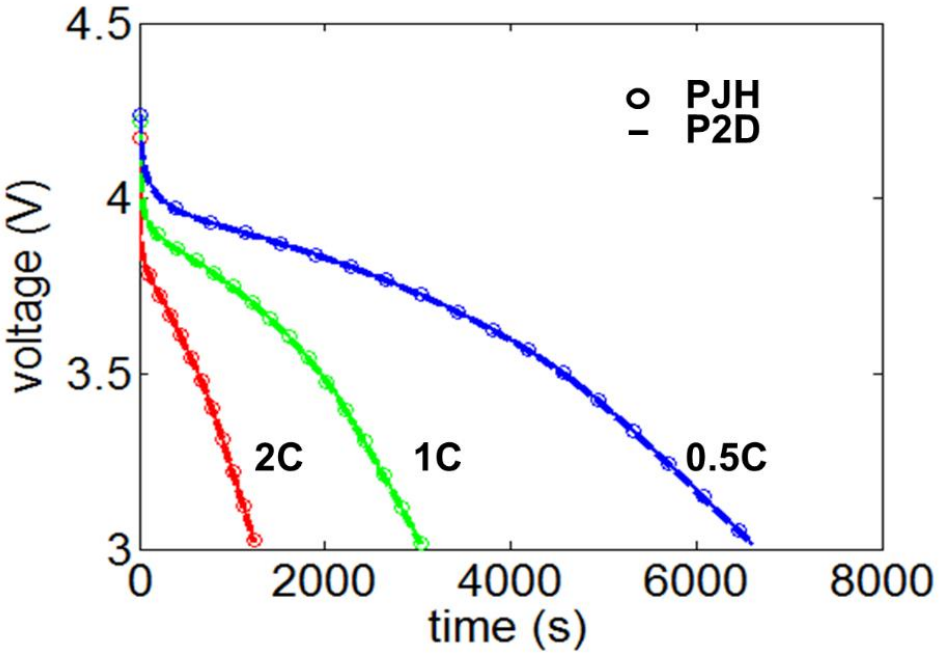

Figure 1. Discharge Voltage profile of PJH and P2D model at different c-rate.

Figure 2 shows the concentration profile from both the model (P2D and PJH) at different time at different locations. The concentration at the solid is almost identical from

both model. In summary, the proposed approach well demonstrate the cell behavior and are well matched with the conventional pseudo-2D model.

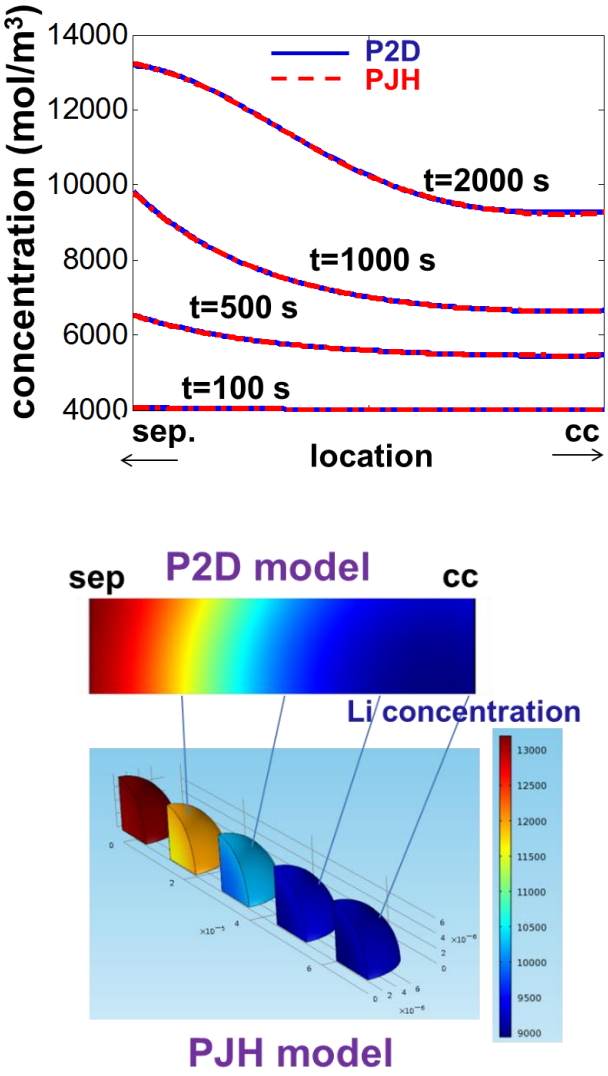

Figure 2. (a) Solid phase concentration profiles at various times; (b) the concentration in the solid phase at the surface of the particle at various times.

3.2. POINT-JUNCTION HIERARCHICAL MODEL

To test the model, a COMSOL simulation was run describing a 1C discharge of the battery. The test was run until the electrode potential at the cathodic current collector was

less than 3.00 Volts. A series of tests were run where the grain boundary diffusion coefficient was 10,000 times larger than the diffusion coefficient of the bulk material. In each of the new tests, the 3D quarter spheres were linked to different places on the 1D electrode model, meaning that several permutations of the grain boundary test were run. This was done because the geometry of grain boundaries is probabilistic in nature, and the order switching elucidates the effect that variable geometry can produce with respect to best and worst case scenarios and general trends. In order to better separate and understand the nature how material properties interact with grain boundary diffusion, the 104 diffusion ratio was used with only one electrode at a time. The cathode was tested first in order to find configurations that gave the highest and lowest maximum stress states.

Figure 3 is a graph that displays the maximum stress in the cathode at any given time. The stress of interest being the first principle stress, as it is a preferred indicator of failure in brittle materials. The grainless model has negligible grain boundary diffusion, and the numbered runs represent the permutation of particle geometries used. The 12345 permutation, coincidentally the configuration with the least amount of stress reduction, signifies the original ordering of the particles, where the first and fifth particles in the 3D model respectively correspond to the first position (separator) and fifth position (collector) on the 1D model. The 25134, with the highest stress reduction, denotes the permutation where the second particle is put into the first position and the fourth particle is put into the fifth position. It is important to note these critical permutations are not an indication of the maximum or minimum stress reductions achievable, they are the maximum and minimum stress reductions achieved from a test of five permutations for a given Voronoi seed.

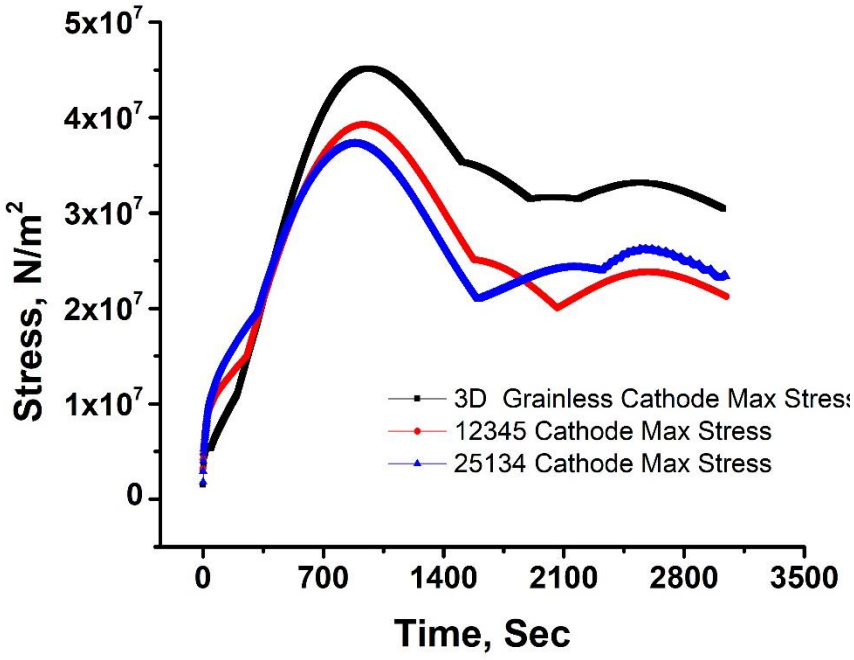

Figure 3. Maximum principle stress in the cathode as a function of time for critical grain configurations.

The results show that, depending on the permutation, the magnitude of the maximum stress profiles vary noticeably. Despite the variability, all diffusive grain boundary runs had significantly reduced induced stresses compared to the featureless model. Since the run was also run at constant current, the increase in elapsed time is equivalent to an increase in battery capacity. Without any grain boundary diffusion the elapsed time was 3030 seconds. Adding diffusion to the cathode gave a marginally improved time of 3049 seconds for the 12345 case and 3046 seconds for the 25134 case. Since particle grain boundary in a real system varies across the width of the electrode, the variability between permutations in an extensive property such as capacity has much less importance than that of an intensive property such as stress. These critical orientations were then mirrored across the center of the separator and applied to the anode, so that the same

particle geometries for the separator and current collector would be the same for both the cathode and anode. These critical orientations are referred to as 12345m and 25134m. The anode grain diffusion ratio was set to 104 without cathode grain boundary diffusion, and the simulation was run at the same discharge current. The stress results are given in Figure 4.

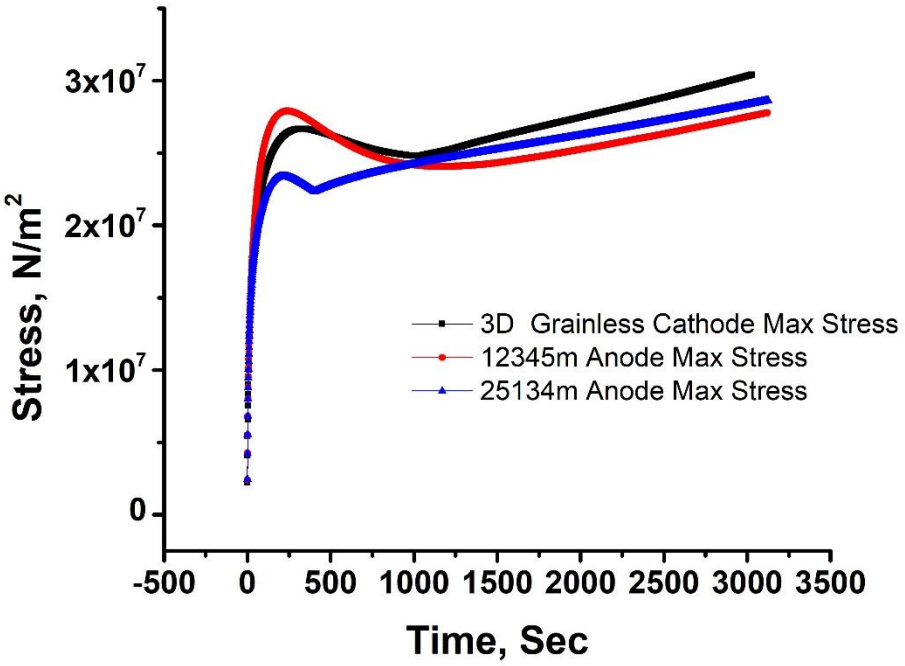

Figure 4. Maximum principle stress in the anode as a function of time for mirrored grain configurations.

In some ways the stress profiles for the mirrored configurations in the anode resemble yet diverge from their cathode counterparts. In the long term, both grained configurations led to a decrease in net stress compared to the ungrained case. Similarly, the 12345m initially has higher stress than the 25134m case, but this relationship reverses during the charge process. However, the 25134m case shows a sharp cusp behavior not present in the other cases, and the 12345m has an initial stress peak that exceeds the

grainless case. The 12345m and 25134m cases led to a discharge duration of 3122 and 3126 seconds, respectively. This suggests the anode grain boundary behavior plays a much more beneficial role in increasing capacity than the specific geometry of the grain boundary.

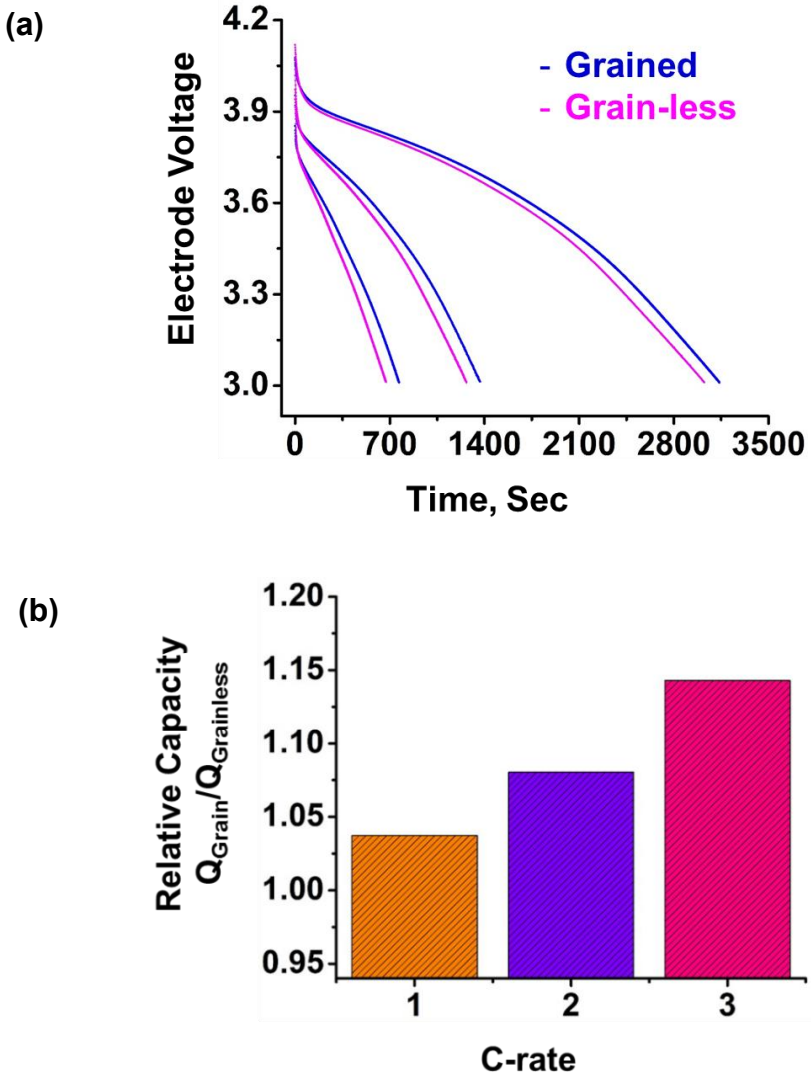

Figure 5. (a) Cell discharge behavior for grained vs grain- less at different c-rate, (b) Cell capacity utilization of grained structure vs grain-less at different c-rate.

The voltage profiles of the cell during discharge are given in Figure 5a. Figure 5b shows that the inclusion of grain boundary increases the cell-capacity utilization compared to that of the grain-less structure.

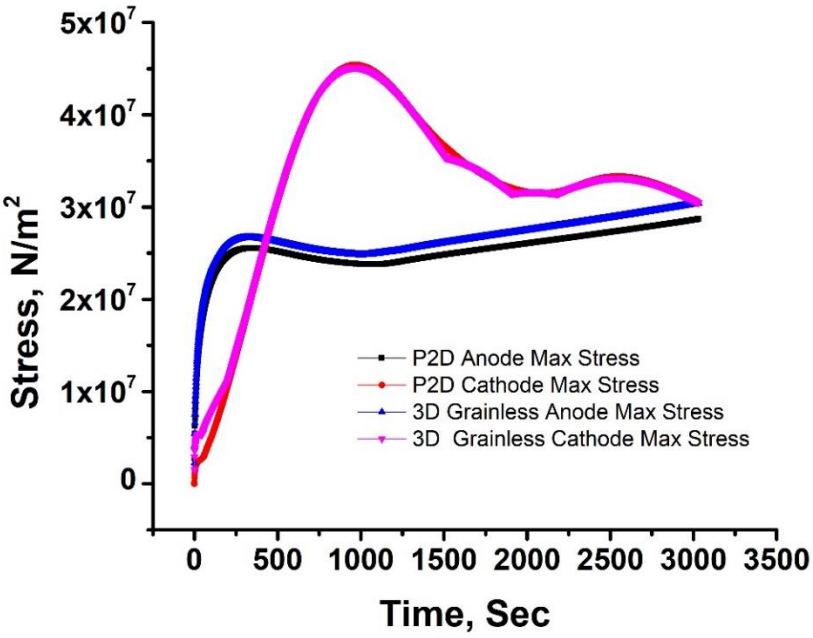

Figure 6. PJH vs P2D stress profiles.

In order to validate the model used, a grain-less point-junction hierarchical model was run against a P2D model that incorporated stress generation. Both models suggested similar stress profiles. The PJH anode stress predicted is higher than the P2D predicted stress. This can be attributed to the fact maximum tensile stress occurs at the outside of a spherical particle in the anode and on the inside in the cathode during discharge: the approximation of a spherical geometry by polygonal finite elements affects stress calculation at the former much more severely than the latter. The refinement of the mesh reduced this variation. The cathode stress profiles showed strong agreement in magnitude,

but the PJH profile showed cusp like behavior not reflected in the P2D profile. The comparison is shown in Figure 6.

In order to examine further the effects grain boundary diffusion can play on stress and capacity, the highly diffusive grained model was run against the grainless model for various C-rates. The results for the anode maximum stress are shown in Figure 7 and the results for the cathode maximum stress are shown in Figure 8.

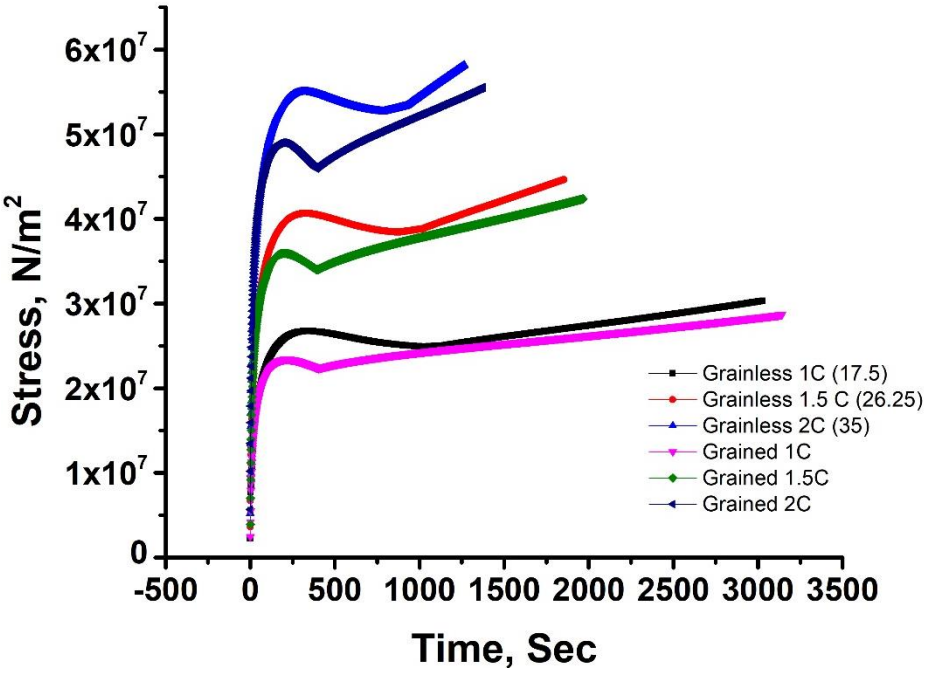

Figure 7. Maximum anode stress versus time for multiple discharge rates.

The anode shows a more consistent behavior: as current increases, stress increases with roughly exponential proportionality with profiles showing similar shape. The gap between the grained stress profiles and the grainless profiles also increases. Thus, it appears that for the anode, the grain effect on stress for an increased current is easily estimable from the stress profile of a lower current. The cathode, however, shows much variation as current increases. The grainless profiles start to change shape at 2C.

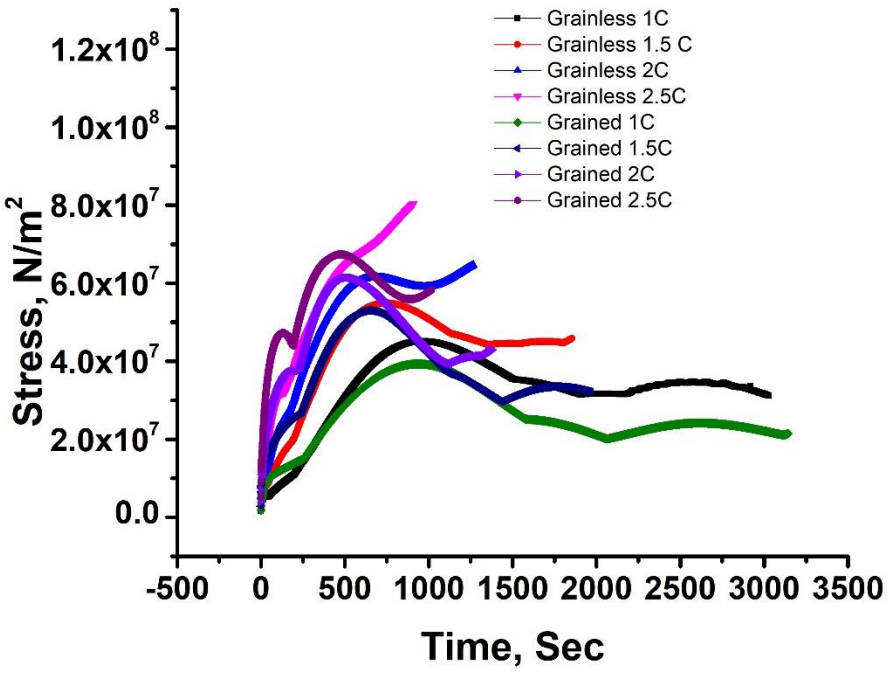

Figure 8. Maximum cathode stress versus time for multiple discharge rates.

4. DISCUSSION

It is also important to note the location where the maximum stress occurs. Intuition dictates that the location of the maximum stress state will always be at the location of maximum localized ion flux. It is often assumed that the local current density should be maximum where the electrode meets the separator. Early work that supports this hypothesis consists of analytical solutions for the initial and steady state for adsorption based electrodes. In testing the P2D model, these assumptions are not completely untrue, as the location of the total maximum cathodic tensile stress (the first peak) occurs at the separator. The stress behavior is also shown to be closely related to the flux. The issue, however, is some time after that peak, the location of maximum stress begins moving toward the

current collector. The cell scale ion flux profile mirrors this change, originally maximum near the separator before moving towards the current collector. Interestingly, near the end of discharge, the stress and flux starts increasing near the separator again. The reason for the cusp like behavior in the PJH is because the continuum maximum stress occurs at a location between the particles being examined. On the P2D anode side, the location of maximum stress was always at the separator. However, the location of maximum ion flux shifted from the separator to the collector much more gradually than in the cathode. While ions are initially predisposed towards maximum influx near the separator, the accumulation of ions at the surface of the electrode resist further flux. While the ions may have to travel physically further through the electrolyte, the lower surface concentration further along the electrode makes that location the path of least resistance. Furthermore, in the grained model, where each particle has varying heterogenous diffusion paths, the location of maximum stress in the anode changed in the 25134m case, indicated by the sharp cusp behavior. In the 25134m case, the highest stress initially took place at the particle near the separator, but eventually switched over to the same particle that was closest to the separator in the 12345m case. With that knowledge, the reason why maximum stress, in the long term, in the 25134m case exceeds that of the 12345m case: the particle with a lower effective diffusivity than the particle at the separator eventually undergoes higher flux than the particle at the separator. When particles are homogeneous and have the same effective diffusivity, the gradual change of the flux profile is apparently not enough to change the location of maximum stress as the stress is dependent on the time history of the flux profile. But when there are particles with different effective diffusivity, then the stress is going to be higher at those locations, always or eventually. Given that any real system is going to

have a mix of particles of varying effective diffusivities located at the same position of a cell, then the stress profiles of the 12345m and 25134m can be considered to be occurring simultaneously. Thus, it appears effective diffusivity of a particle outweighs its location on the electrode for the anode.

Regarding the Cathodic response to increasing current, the profile change could prove significant. From the reduction in cusps, we can infer that the location of maximum stress is likely not moving from one particle to the next. This link between stress profile shape and input current concurs with previous work. At some point, increasing input current causes stress evolution to remain at the separator. The previous work indicated that this stress profile emerged when current was increased from 1C to 10C. [2] This suggests that the location of maximum stress is variable for lower currents, possibly important for applications where long life and low-output are expected.

5. CONCLUSION

These simulations confirm that the location of the maximum stress in an electrode at a given time varies throughout the length of the electrode. However, these simulations also suggest that the profile is variable and that the location of maximum stress over all time may or may not occur at the separator interface. This variability might be attributed to the choice of parameters. While the separator interface is indeed a point of interest, it seems that it alone is not sufficient to evaluate or manage electrode life.

Furthermore, the presence of grain boundaries appears to provide an overall ameliorating effect of reducing maximum stress in the electrode. Influencing the formation

of grain boundaries could provide a crucial element in providing for higher performance batteries while maintaining acceptable life and cycling. The variability in grain structure also appears to contribute strongly to stress generated: less diffusive particles near the back could suffer more damage than more diffusive particles near the front. Considering this variability with the varying maximum stress location, if some form of progressive damage analysis is to be done, it is necessary to consider the whole electrode. Assuredly, the existence of diffusion-enhancing boundaries significantly reduces the predicted stresses in the electrode. This suggests that while effects of the grain boundary might be negligible for determining electrical performance, they cannot be neglected for determining loading that the material receives from charging and discharging. This is an important consideration for any kind of determination of mechanical degradation as it reveals that assuming a perfectly spherical, homogenous (one-dimensional) model of particle concentration cannot be used to determine stressing (at least not without some correction factor).

It is important to note that in order to understand if the models that were developed more accurately portray the behavior of real life batteries, then experiments need to be done. The voltage-time data is easier to obtain, but the model predicts that this should not be too different from previous models which behave closely to experimental values, and thus is not as critical to testing. The reduction in induced stress, while more important to validating the model, is harder to test due to the scale of the material to be tested.

ACKNOWLEDGEMENTS

The authors thank University of Missouri system for support.

REFERENCES

[1] T. Mütschele, R. Kirchheim, Segregation and diffusion of hydrogen in grain boundaries of palladium, Scr. Metall. 21 (1987) 135–140. doi:10.1016/0036-9748(87)90423-6.

[2] W. Sprengel, Diffusion in Nanocrystalline Materials, Nanostructured Mater. Process. Prop. Appl. Second Ed. 62 (2006) 331–364. doi:10.1016/B978-081551534-0.50010-5.

[3] G.P. Grabovetskaya, M.B. Ivanov, A.P. Zhilyaev, R.Z. Valiev, Grain Boundary Diffusion Characteristics of, Scr. Mater. 44 (2001) 873–878.

[4] W.S. Kim, Characteristics of LiCoO2 thin film cathodes according to the annealing ambient for the post-annealing process, J. Power Sources. 134 (2004) 103–109. doi:10.1016/j.jpowsour.2004.02.035.

[5] S.C. Mui, J. Jasinski, V.J. Leppert, M. Mitome, D.R. Sadoway, A.M. Mayes, Microstructure Effects on the Electrochemical Kinetics of Vanadium Pentoxide Thin-Film Cathodes, J. Electrochem. Soc. 153 (2006) A1372. doi:10.1149/1.2199327.

[6] J. C. Fisher, Calculation of Diffusion Penetration Curves for Surface and Grain Boundary Diffusion, J. Appl. Phys. 22 (1951) 74–77.

[7] S. V. Divinski, G. Reglitz, G. Wilde, Grain boundary self-diffusion in polycrystalline nickel of different purity levels, Acta Mater. 58 (2010) 386–395. doi:10.1016/j.actamat.2009.09.015.

[8] Y. Mishin, M. Asta, J. Li, Atomistic modeling of interfaces and their impact on microstructure and properties, Acta Mater. 58 (2010) 1117–1151. doi:10.1016/j.actamat.2009.10.049.

[9] Y.-C. Chung, C.K. Kim, B.J. Wuensch, Calculation of the contribution to grain boundary diffusion in ionic systems that arises from enhanced defect concentrations adjacent to the boundary, J. Appl. Phys. 87 (2000) 2747. doi:10.1063/1.372250.

[10] D. Gryaznov, J. Fleig, J. Maier, Numerical Study of Grain Boundary Diffusion in Nanocrystalline Materials, Defect Diffus. Forum. 237–240 (2005) 1043–1048. doi:10.4028/www.scientific.net/DDF.237-240.1043.

[11] W. Preis, W. Sitte, Modeling of fast diffusion along grain boundaries in oxide ceramics, Solid State Ionics. 179 (2008) 765–770. doi:10.1016/j.ssi.2007.12.103.

[12] H. Jung, M. Park, Y.G. Yoon, G.B. Kim, S.K. Joo, Amorphous silicon anode for lithium-ion rechargeable batteries, J. Power Sources. 115 (2003) 346–351. doi:10.1016/S0378-7753(02)00707-3.

[13] S. Han, J. Park, W. Lu, A.M. Sastry, Numerical study of grain boundary effect on Li+ effective diffusivity and intercalation-induced stresses in Li-ion battery active materials, J. Power Sources. 240 (2013) 155–167. doi:10.1016/j.jpowsour.2013.03.135.

[14] Y. Dai, L. Cai, R.E. White, Simulation and analysis of stress in a Li-ion battery with a blended LiMn2O4 and LiNi0.8Co0.15Al0.05O2 cathode, J. Power Sources. 247 (2014) 365–376. doi:10.1016/j.jpowsour.2013.08.113.

III. SYNTHESIS OF NANO-FIBROUS NICKEL COCOONED VO_x ANODE FOR HIGH PERFORMANCE LI ION BATTERY

Susmita Sarkar[1], Jonghyun Park[1,*]

[1]Department of Mechanical Engineering, Missouri University of Science and Technology, Rolla, MO 65409, United States

*Corresponding author Email: parkjonghy@mst.edu

ABSTRACT

Owing to the high energy density and long cycle life, lithium-ion batteries are the state of the art for electric vehicles and other large scale-energy storage device. The demand for high cell stability and reversibility has increased the attention toward conversation type of anode materials than the intercalation-type of materials. Conversion based material can achieve significantly higher initial capacity as they can use more lithium ion during charging/discharging process. In the case of conversion based material, there is always a trade-off such as higher initial specific capacity and poor reversibility. So a few elements mainly oxides from periodic table found only a limited measure of success so far. Herein we report the development of high performance fiber based flexible li ion battery based on Ni-VO_x-CNF anode. Even though vanadium oxide based electrode has lot of advantages like low cost, abundance and high theoretical capacity, the disadvantages like slow lithium ion diffusion, poor cycling stability and low electrical conductivity makes it an unpromising anode material. The use of electrospinning approach overcomes all these issues and the addition of Ni matrix ensure the negligible capacity loss and higher cycling stability.

The rapid development of electric vehicles (EV) and plug in hybrid EVs, vitalized the extensive research for new advanced electrodes materials with the benefits of high cycling stability, high energy and power density. Earnest efforts have been made to improve the electrodes especially cathode by using new type of materials or by modifying architectures. However, as far as anode side is concerned, carbonaceous graphite is still the dominant anode material. Low theoretical capacity (372 mAh/g) of this material on the way of its application in high energy battery. To enhance the capacity, it is necessary to overcome the intrinsic limits of the intercalation type of anode materials which can accommodate Li per transition metal core. To breakthrough this obstruction, uses of materials which is capable of accommodating more than one Li ion during charging/discharging process has been proposed. Transition metal oxides based on conversion chemistry have been regarded as a promising alternative to the intercalation anode materials. Vandium based compounds with multi electron reaction such as VO_2,[1] V_2O_5,[2–4] $FeVO_4$, ZnV_2O_4,[5] Li_3VO_4,[6] $LiVMoO_6$,[7] V_2O_3 [8,9]and $Li_{1+x}VO_2$ [10]etc. have been studied for higher lithium ion insertion content providing larger specific capacity.

Among the diversified candidates investigated, V_2O_5 attract most of the attention owing to their higher specific capacity and higher electrochemical potential, all being resulted from the many accessible oxidation states of vanadium. Fascinatingly V_2O_5 can be used both as cathode and anode. V_2O_5 has great promises to be used as high energy anode as it holds theoretical capacity of 1472 mAh/g for a full reduction of V^{5+} to metallic V^{0+}. Still, a little effort has been made to use this material for stable electrochemical

performance. It has been shown that V_2O_5 aerogels showed a capacity of 100 mAh/g after 30 cycles at a rate of 118 mA/g. Also, V_2O_5 with SnO_2 showed capacity of 600 mAh/g after 50 cycles. Inspired by that, Zhang et al reported V_2O_5 -C-SnO_2 hybrid nanobelts which displayed a high reversible capacity of 930 mAh/g after 50 cycles at a rate of 200 mA/g.[4] Generally, thermal processing with carbon can easily reduce higher valence (+5 or +4) to lower valence compounds. More recently, Li_3VO_4 has been introduced as a potential anode with a discharge capacity of 738.5 mAh/g.[6]

In the conventional slurry casting process, a high content of polymer binder and conductive additives are needed along with the active material to enable a stable cycling. From the architectural aspect, the conventional LIB electrodes are blending of active materials, conductive agents such as carbon black and polymer binders spread over a metallic foil current collector and the performance of the cell highly depends on the electrode thickness, amount of active material and porosity. Current collector, binder and carbon black are inactive masses and do not participate in electrochemical reactions. However, this unsatisfactorily decreases the energy density due to the excessive non-active materials used to maintain a good cell performance. Thus, thinner foil and lesser binder and conductive agents are expected for high energy density performance. However, lowering these inactive masses comes with a cost. For example, lower amount of binder will cause structural dis-integrity during li insertion/de-insertion process and lower carbon black will decrease the conductivity and thus causing poor cell performance. Furthermore, the active mass loading of convention slurry casted electrode cannot be increase as they tend to become less conductive with higher thickness.

To mitigate these issues, uses of highly conductive carbon-based nanofibers instead of stacked up electrodes is an attractive approach. Carbon fibers can not only hold up the structure, also possess a comparable electrochemical stability to Al/Cu foil and thus eliminating the needs of extra binders, conductive agents and current collector. Nanofibers has unique property which can shorten the ion diffusion path, their high area/mass ration allows faster lithium intercalation kinetics. Electrospinning is a cost effective and continuous material approach for continuous long nano-fibers. In this work, VO_x -CNF and Ni wrapped VO_x-CNF fibers were synthesized directly as a self-supporting non-woven mat of nanofibers with the aid of heat treatment excluding the necessity for extra binders or slurry processing. They were device-ready and were directly incorporated into the Li-ion coin cell as anode material.

In this paper, we fabricated a new Ni- VO_x -Carbon nanofiber (CNF) and utilized it as an anode material in Li ion battery. The synthesis steps includes producing VO_x composite nanofibers based on electrospinning process. In the process, first V_2O_5 powder was mixed with polymer powders (PAN and PVP) and then adequate amount of DMF was added to the mixture and stirred it for 12 hrs. Also, another batches were prepared with 3 wt % of Ni and 5 wt% Ni added into the mixture. The homogenous mixture was then added into a syringe and deposited the fiber in an aluminum current collector with the application of electric voltage. After the fiber was obtained, those were peeled off from the substrate and then a calcination process was carried out in N_2 atmosphere at 800^0C to convert the polymer precursors to carbon fibers. During the same time, presence of excess carbon at high temperature partially reduced V_2O_5 to V_2O_3 and VO_2 without destroying the fiber

structure. This Ni- VO_x –CNF composite possessed significant improvement in capacity, rate capability and improved cycling life.

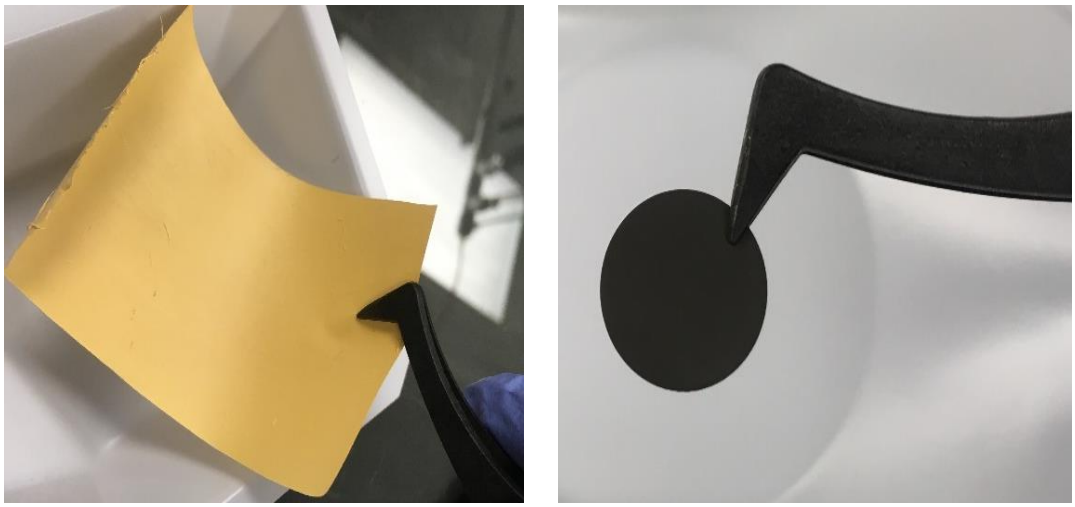

Figure 1. Free standing V_2O_5 nanofibers (a) as-spun and (b) after the calcination at 800^0C. Calcinated fibers has good flexibility and used as it is the anode for the li ion battery.

Figure 1a (Digital Image) shows the as spun V_2O_5 fibers which was peeled off from the aluminum foil as a free standing nanofiber mat. Figure 1b shows the calcinated nano-fiber mat after heating at 800^0C at N_2 atmosphere. Before application of high temperature, a stabilization process was carried out at 270^0C to keep the structure of the fiber mat. Figure 2 shows typical SEM images of the fibers V_2O_5 and Ni added-V_2O_5 fibers. Long nanofibers with uniform diameter were observed. The fibers are of few hundred nanometer in diameter. Pure PAN-PVP nanofibers were also produced and they didn't show any beading with the fibers. However, addition of V_2O_5 and Ni causes some beading along with the electrospun fibers. The average diameter of the calcinated nanofibers became smaller due to the weight loss during carbonization process. However, the fiber shape and regularity was maintained even after the calcination.

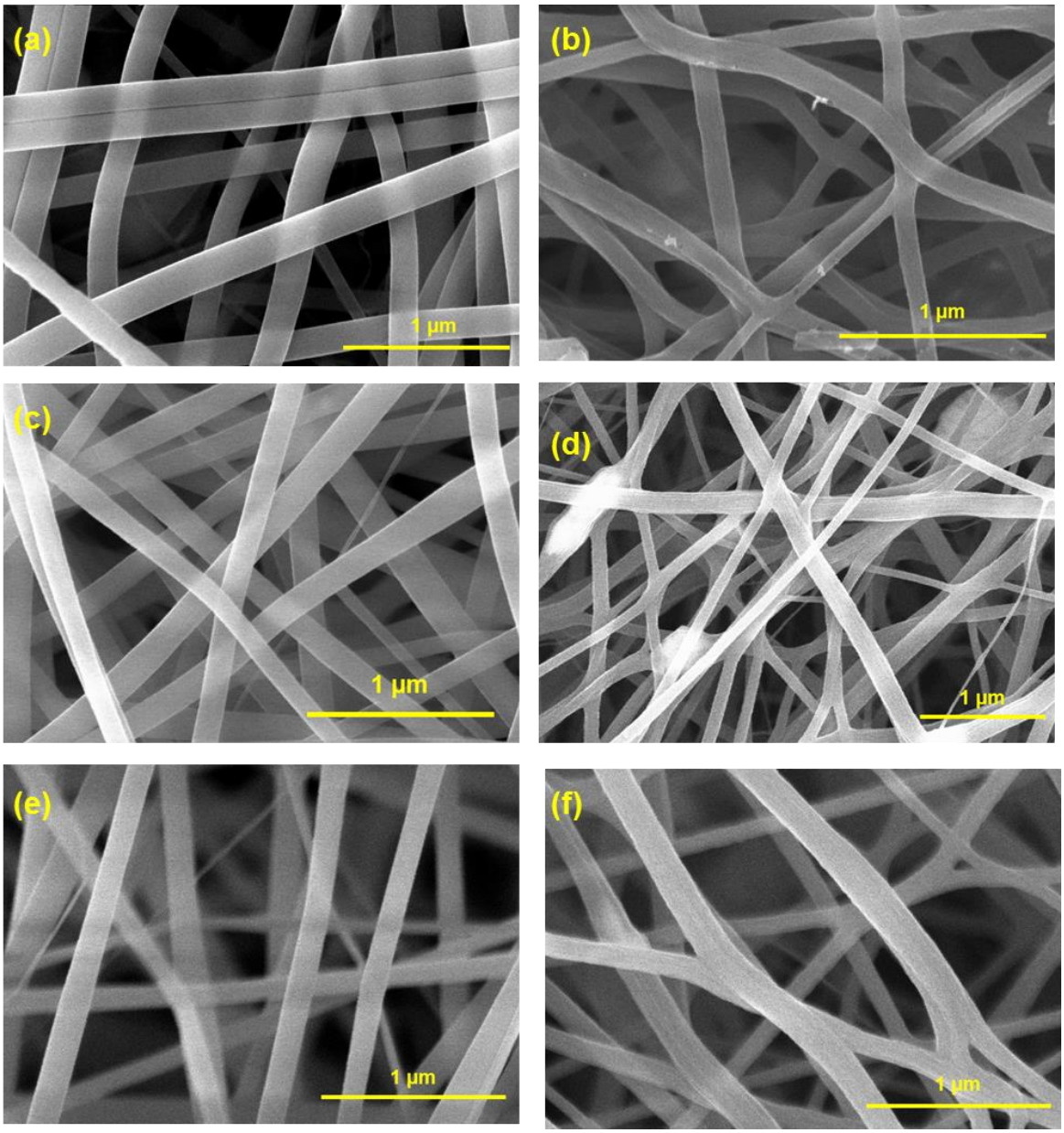

Figure 2. SEM images of (a) as-spun V_2O_5 nanofibers, (b) calcinated V_2O_5 nanofibers, (c) as-spun 3wt% Ni-V_2O_5 nanofibers, (d) calcinated 3wt% Ni-V_2O_5 nanofibers, (e) as-spun 5wt% Ni-V_2O_5 nanofibers and (f) calcinated 5wt% Ni-V_2O_5 nanofibers.

Figure 3 represents the XRD pattern of the as-spun V_2O_5 and calcinated pure V_2O_5 and with Ni additives. By indexing the peaks we can ascribe them to pure V_2O_5 peaks for as-spun fibers. However, after the calcination the combination peaks of VO_2 (JCPDS: 65-

7960) and V_2O_3 (JCPDS: 34-0187) appears for all the cases. No peaks due to V_2O_5 were detected for calcinated samples. The thermal decomposition of V_2O_5 at elevated temperatures were studied previously. It was shown that with the increment in heating temperature a sequence of transformations from V_2O_5 via VO_2 to V_2O_3 occurs. [11]

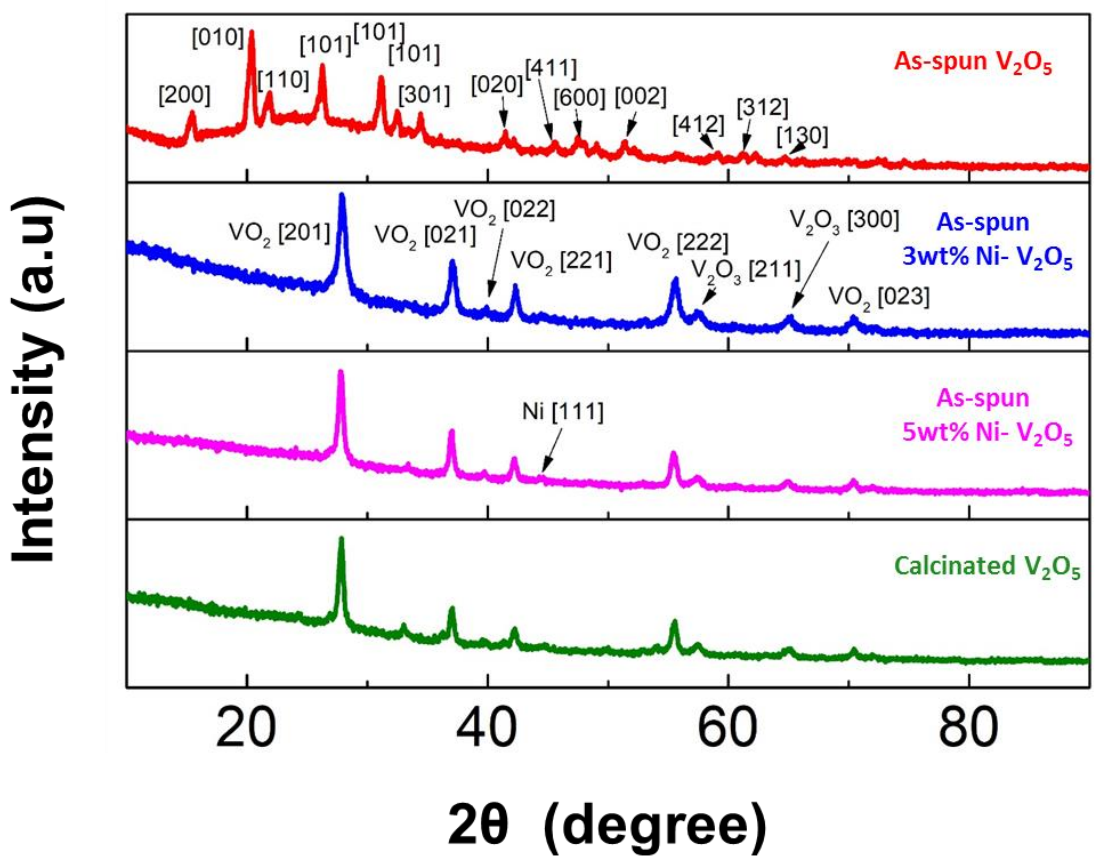

Figure 3. XRD patterns of (a) As-spun V_2O_5 (b) Calcinated- 3wt% Ni-V_2O_5, (c) Calcinated- 3wt% Ni-V_2O_5 nanofiber electrodes and (d) Calcinated-V_2O_5 electrodes.

The outer carbon layer derives from the polymer precursors of fibers also helps in reducing the V_2O_5 to V_2O_3.[8]

$$V_2O_5 + C \rightarrow V_2O_3 + CO_2 \quad (1)$$

V_2O_3 nanocomposite has already shown a great promises as anode in li-ion battery. Addition of outer carbon layer outside the VO_x particles favors the electrode kinetics by providing a charge transport channel. These unique characteristics are perfect for a li-ion battery with high rate capability and high stability. Ni insertion into a V_2O_5 lattice improved the electrochemical reactions of cathode material by offering the electric stability to the V^{4+} state.[12] Thus introduction of Ni into the nanofiber matrix are expected to improve the cell performance notably.

V_2O_3 is a multi-functional material which has a theoretical capacity around 1070 mAh/g, much higher than commercialized graphite material. Also, VO_2 is another attractive anode material. VO_2 with graphene showed a high reversible capacity of 400 mAh/g over 400 cycles in a large window of 0.05–3.0 V.[1] The discharge curves for the micro-sized vanadium pentoxide particles and the variation of discharge capacity versus cycle number plots are shown in Figure. 4. It shows the charge–discharge profiles on various cycles obtained at 100 mAh/g between 3 and 0.01 V. All discharge curves display a slightly sloping plateau from 2.4 V to 2 V, followed by a well-defined at plateau at 1.9 V. In the mixture of the V_2O_3 and VO_2, VO_2 is the dominating phase. Thus the capacity obtained is near the theoretical value of VO_2. The plateaus are progressively diminished and evolved to sloping plateaus after 1st cycle. For electrode with pure V_2O_5 as starting material has an initial capacity around ~586 mAh/g. The discharge capacity on the 2^{nd} and 10^{th} cycle is ~299 mAh/g and 311 mAh/g at 100 mA/g current. It is interesting to note that the addition of Ni has improved the capacity significantly. With the addition of 3 wt% and 5wt% Ni, the first capacity obtained was ~637 mAh/g and ~768 mAh/g, respectively. The discharge capacity for 3wt% Ni-V2O5 on the 2^{nd} and 10^{th} cycle is ~324 mAh/g and ~327

mAh/g at 100 mA/g current. The discharge capacity for 5wt% Ni-V_2O_5 on the 2nd and 10th cycle is ~456 mAh/g and 472 mAh/g at 100 mA/g current.

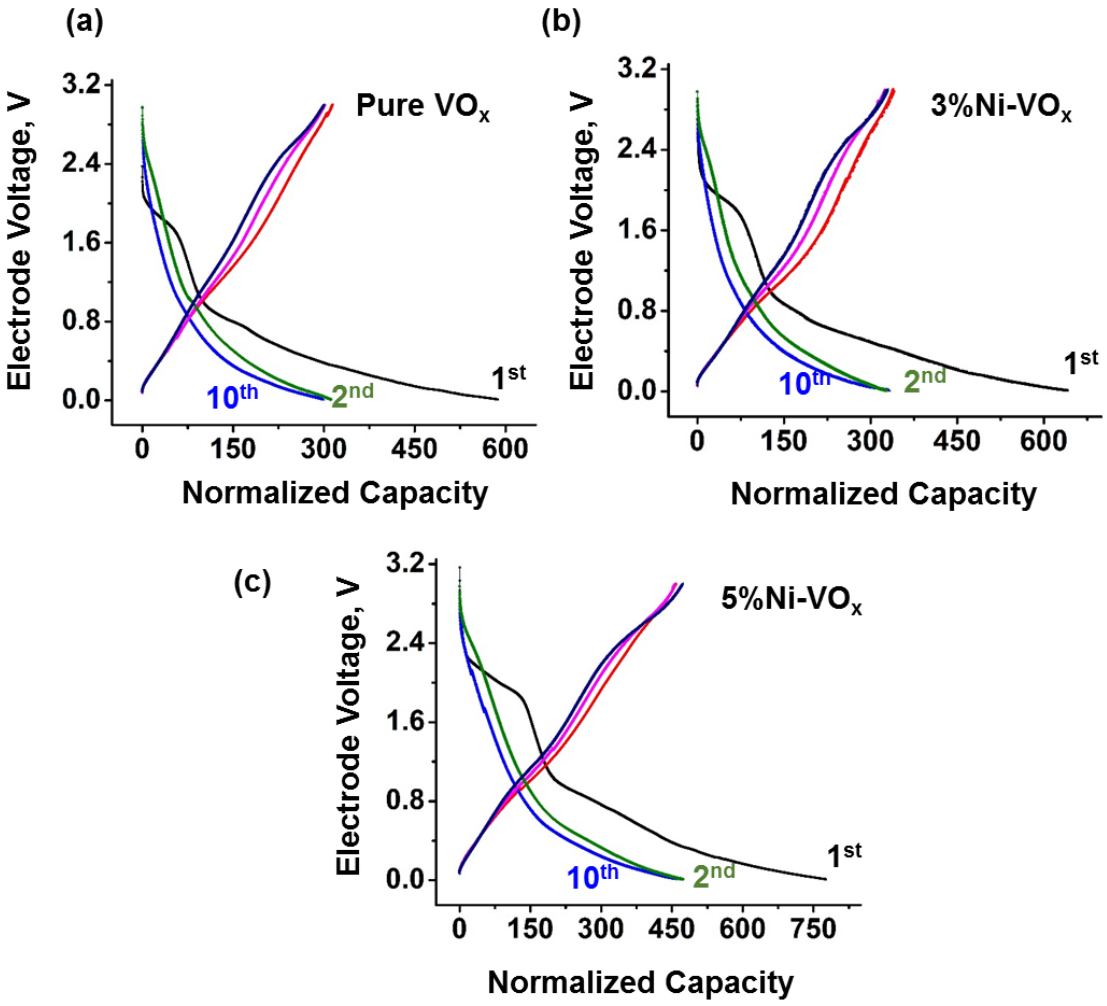

Figure 4. Discharge Voltage profiles for (a) V_2O_5 (b) 3wt% Ni-V_2O_5 and (c) 3wt% Ni-V_2O_5 nanofiber electrodes.V_2O_5 with 3 wt% Ni particle shows significant cycle life improvement than the other electrodes.

The reversibility and recoverability of all the fibrous sample can be observed form the figure 5. Such a high reversibility and cycling stability can be seen for few material with higher amount conductive agent present. Our method totally eliminate the need of

additional conductive agent and still showing such a stably cyclic performance from the 2nd cycle onwards.

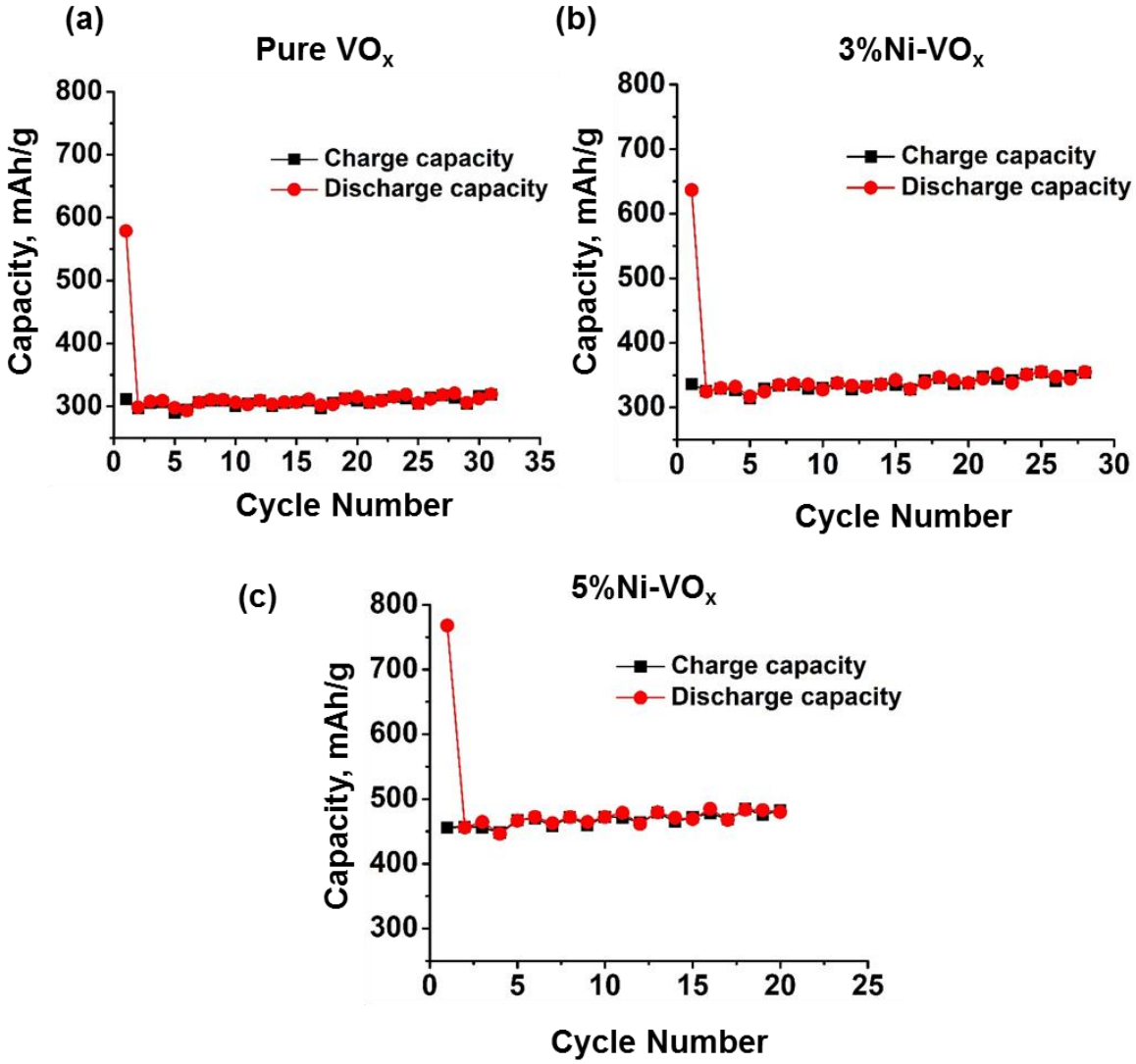

Figure 5. Cyclability demonstration for (a) V_2O_5 (b) 3wt% Ni- V_2O_5 and (c) 3wt% Ni-V_2O_5 nanofiber electrodes. All the sample shows stability from the 2nd cycle.

VO_2 or V_3O_4 is rarely used anode material for li ion battery because of its poor conductivity and metastability. In this work a composite of VO_x and carbon nanofiber has been successfully fabricated without the need of additional binders or conductive agent. The outstanding performance of the porous nanofibrous anode can be attributed to the

conductive carbon nanofiber material and the electroactive Ni-VO_x particles. The mechanical stress-strain has been effectively suppressed by the incorporation of the porous fibers and the presence of Ni-matrix in the electrode. Rapid li ion diffusion between the electrode and electrolyte is also one of the major causes for the improved performance.

In conclusion, we have successfully produced a Ni-VO_x nanofibers accompanied by carbon nanofibers for anode material of li-ion battery. The as-prepared fibers can be directly used in the coin cell fabrication without the need of additional active masses and thus increasing the solid loading of the electrodes significantly without compromising the cell performance. Extraordinary cell performance, reversibility, low-toxicity and abundance, make this composite nanofiber an ideal anode material for advanced li-ion battery.

1. ASSOCIATED CONTENT

1.1. SUPPORTING INFORMATION

1.1.1. Synthesis of V_2O_5 and Ni Wrapped Fibers. The solution was prepared by mixing V_2O_5 micropowder in DMF solvent under stirring at 80^0C for 12 hrs. Another solution was prepared by mixing PAN and PVP in DMF solvent. Both of the solutions were mixed together for 12 hrs to obtain a homogeneous and spinnable solution. For the other two samples, 3 wt% and 5 wt% of Ni was added to the previous solution respectively. Then the fibers were first stabilized at 120^0C and then calcinated at 800^0C for 1 hr.

1.1.2. Electrochemical Tests. The dried electrodes had approximately ~5-6 mg electrochemically active material. Li metal anodes were prepared from a 0.75 mm-thick ribbon (Aldrich), and 1 M solution of $LiPF_6$ in EC: DMC served as the electrolyte. Coin

type cells were built in an Ar filled glove-box.Galvanostatic measurements were performed in the voltage range of 0.01–3.0 V at 100 mA/g. The reported specific capacities were calculated based on the total mass of the fibers.

2. AUTHOR INFORMATION

2.1. CORRESPONDING AUTHOR

*****Email: parkjonghy@mst.edu

2.2. NOTES

The author declare no competing financial interest

ACKNLOWLEDGEMENTS

The author wants to thank Dr. Eric Bohmann for helping with XRD.

REFERENCES

[1] G. He, L. Li, A. Manthiram, VO_2 /rGO nanorods as a potential anode for sodium- and lithium-ion batteries, J. Mater. Chem. A. 3 (2015) 14750–14758. doi:10.1039/C5TA03188E.

[2] J. Liu, H. Xia, D. Xue, L. Lu, Double-Shelled Nanocapsules of V 2 O 5 -Based Composites as High-Performance Anode and Cathode Materials for Li Ion Batteries, J. Am. Chem. Soc. (2009) 12086–12087. doi:10.1039/b900116f.

[3] R. Yu, C. Zhang, Q. Meng, Z. Chen, H. Liu, Z. Guo, Facile synthesis of hierarchical networks composed of highly interconnected V2O5 nanosheets assembled on carbon nanotubes and their superior lithium storage properties, ACS Appl. Mater. Interfaces. 5 (2013) 12394–12399. doi:10.1021/am4033444.

[4] L. Zhang, M. Yang, S. Zhang, Z. Wu, A. Amini, Y. Zhang, D. Wang, S. Bao, Z. Lu, N. Wang, C. Cheng, V2O5-C-SnO2 Hybrid Nanobelts as High Performance Anodes for Lithium-ion Batteries, Sci. Rep. 6 (2016) 33597. doi:10.1038/srep33597.

[5] L. Xiao, Y. Zhao, J. Yin, L. Zhang, Clewlike ZnV_2O_4 hollow spheres: Nonaqueous sol-gel synthesis, formation mechanism, and lithium storage properties, Chem. - A Eur. J. 15 (2009) 9442–9450. doi:10.1002/chem.200901328.

[6] Z. Liang, Z. Lin, Y. Zhao, Y. Dong, Q. Kuang, X. Lin, X. Liu, D. Yan, New understanding of Li_3VO_4/C as potential anode for Li-ion batteries: Preparation, structure characterization and lithium insertion mechanism, J. Power Sources. 274 (2015) 345–354. doi:10.1016/j.jpowsour.2014.10.024.

[7] N. Chen, C. Wang, F. Hu, X. Bie, Y. Wei, G. Chen, F. Du, Brannerite-Type Vanadium–Molybdenum Oxide $LiVMoO_6$ as a Promising Anode Material for Lithium-Ion Batteries with High Capacity and Rate Capability, ACS Appl. Mater. Interfaces. 7 (2015) 16117–16123. doi:10.1021/acsami.5b05030.

[8] Y. Wang, H.J. Zhang, A.S. Admar, J. Luo, C.C. Wong, A. Borgna, J. Lin, Improved cyclability of lithium-ion battery anode using encapsulated V2O3 nanostructures in well-graphitized carbon fiber, RSC Adv. 2 (2012) 5748. doi:10.1039/c2ra20472j.

[9] X. An, H. Yang, Y. Wang, Y. Tang, S. Liang, A. Pan, G. Cao, Hydrothermal synthesis of coherent porous V2O3/carbon nanocomposites for high-performance lithium- and sodium-ion batteries, Sci. China Mater. 60 (2017) 717–727. doi:10.1007/s40843-017-9054-0.

[10] J.H. Song, H.J. Park, K.J. Kim, Y.N. Jo, J.S. Kim, Y.U. Jeong, Y.J. Kim, Electrochemical characteristics of lithium vanadate, $Li_{1+x}VO_2$, new anode materials for lithium ion batteries, J. Power Sources. 195 (2010) 6157–6161. doi:10.1016/j.jpowsour.2009.12.103.

[11] D.S. Su, R. Schlögl, Thermal decomposition of divanadium pentoxide V_2O_5: Towards a nanocrystalline V_2O_3 phase, Catal. Letters. 83 (2002) 115–119. doi:10.1023/A:1021042232178.

[12] Y.-Z. Zheng, H. Ding, E. Uchaker, X. Tao, J.-F. Chen, Q. Zhang, G. Cao, Nickel-mediated polyol synthesis of hierarchical V_2O_5 hollow microspheres with enhanced lithium storage properties, J. Mater. Chem. A. 3 (2015) 1979–1985. doi:10.1039/C4TA05500D.

SECTION

3. CONCLUSIONS

With the growing energy crisis, Lithium ion battery is a promising candidate to mitigate the issues. The performance of the cell mostly depends on the electrode properties from chemical, mechanical and structural aspects. The 1st goal of this research is to be able to show the origin of cell improvement with a thin layer of CeO_2 coating. The analysis was done both qualitatively and quantitavely incorporating all the physical and chemical phenomenon during cell cycling. A Multiphysics, Multi-scale simulation was performed to show how different layer of coating will have impact on stress generation, metal-ion dissolution and the cell performance. It was found that a 3nm coating layer has much better performance than bare, 2nm and 5 nm coated particles.

The scope of the second paper is to do advanced study of the effect on grain boundary on the cell-performance. Different grain structures were generated inside the cathode and anode particles, where the grain boundary has higher diffusion co-efficient than the bulk. Thus, the stress profiles for the electrodes with grain structure significantly differs from that of without grain electrodes. Also, it has been that the capacity utilization increases at higher c-rate for the grained structure thanks to their high diffusivity and conductivity.

In the third paper, a flexible, device ready fiber based anode was prepared from V_2O_5 based powder along with polymer solution of PAN and PVP in DMF. Also, a small amount of Ni matrix in the V_2O_5 solution significantly improved the li intercalation capacity. It was found from the XRD that due to the high temperature and excess carbon

originated from the carbonization of polymer causes the V_2O_5 transformation into VO_2 and V_3O_4. The mixed VOx-CNF mats were used as it is after the calcination without the need of extra binder and carbon black. Thus, the active masses for the electrode has been increased significantly. Also, good cyclibility and reversibility has been seen for all the samples. The sample 5 wt% Ni has shown the best initial li-intercalation capacity and also, the capacity retention is excellent.

BIBLIOGRAPHY

[1] Y. Mekonnen, A Review of Cathode and Anode Materials for Lithium-Ion Batteries, (2016) 2–7.

[2] A. Eftekhari, Low voltage anode materials for lithium-ion batteries, Energy Storage Mater. 7 (2017) 157–180. doi:10.1016/j.ensm.2017.01.009.

[3] W. Li, B. Song, A. Manthiram, High-voltage positive electrode materials for lithium-ion batteries, Chem. Soc. Rev. 46 (2017) 3006–3059. doi:10.1039/C6CS00875E.

[4] J.W. Fergus, Recent developments in cathode materials for lithium ion batteries, J. Power Sources. 195 (2010) 939–954. doi:10.1016/j.jpowsour.2009.08.089.

[5] T. Ohzuku, R.J. Brodd, An overview of positive-electrode materials for advanced lithium-ion batteries, J. Power Sources. 174 (2007) 449–456. doi:10.1016/j.jpowsour.2007.06.154.

[6] K. Cao, T. Jin, L. Yang, L. Jiao, Recent progress in conversion reaction metal oxide anodes for Li-ion batteries, Mater. Chem. Front. 1 (2017) 2213–2242. doi:10.1039/C7QM00175D.

[7] M. Winter, J.O.J. Besenhard, M.E. Spahr, P. Novák, Insertion Electrode Materials for Rechargeable Lithium Batteries, Adv. Mater. 10 (1998) 725–763. doi:10.1002/(SICI)1521-4095(199807)10:10<725::AID-ADMA725>3.0.CO;2-Z.

[8] M.G. Verde, L. Baggetto, N. Balke, G.M. Veith, J.K. Seo, Z. Wang, Y.S. Meng, Elucidating the Phase Transformation of $Li_4Ti_5O_{12}$ Lithiation at the Nanoscale, ACS Nano. 10 (2016) 4312–4321. doi:10.1021/acsnano.5b07875.

[9] W. Li, X. Sun, Y. Yu, Si-, Ge-, Sn-Based Anode Materials for Lithium-Ion Batteries: From Structure Design to Electrochemical Performance, Small Methods. 1 (2017) 1600037. doi:10.1002/smtd.201600037.

[10] H. Tian, F. Xin, X. Wang, W. He, W. Han, High capacity group-IV elements (Si, Ge, Sn) based anodes for lithium-ion batteries, J. Mater. 1 (2015) 153–169. doi:10.1016/j.jmat.2015.06.002.

[11] Y. Jin, B. Zhu, Z. Lu, N. Liu, J. Zhu, Challenges and Recent Progress in the Development of Si Anodes for Lithium-Ion Battery, Adv. Energy Mater. 1700715 (2017) 1–17. doi:10.1002/aenm.201700715.

[12] J.-Y. Li, Q. Xu, G. Li, Y.-X. Yin, L.-J. Wan, Y.-G. Guo, Research progress regarding Si-based anode materials towards practical application in high energy density Li-ion batteries, Mater. Chem. Front. (2017) 1691–1708. doi:10.1039/C6QM00302H.

[13] R.L. Patel, S.A. Palaparty, X. Liang, Ultrathin Conductive CeO_2 Coating for Significant Improvement in Electrochemical Performance of $LiMn_{1.5}Ni_{0.5}O_4$ Cathode Materials, J. Electrochem. Soc. 164 (2017) A6236–A6243. doi:10.1149/2.0371701jes.

[14] J.H. Woo, J.J. Travis, S.M. George, S.-H. Lee, Utilization of Al2O3 Atomic Layer Deposition for Li Ion Pathways in Solid State Li Batteries, J. Electrochem. Soc. 162 (2014) A344–A349. doi:10.1149/2.0441503jes.

[15] J. Zhao, Y. Wang, Atomic layer deposition of epitaxial ZrO2coating on LiMn2O4nanoparticles for high-rate lithium ion batteries at elevated temperature, Nano Energy. 2 (2013) 882–889. doi:10.1016/j.nanoen.2013.03.005.

[16] R.L. Patel, J. Park, X. Liang, Ionic and electronic conductivities of atomic layer deposition thin film coated lithium ion battery cathode particles, RSC Adv. 6 (2016) 98768–98776. doi:10.1039/C6RA20829K.

[17] L.A. Riley, Atomic Layer Deposition for Improved Electrochemical Stability for Lithium Ion Batteries, Spectroscopy. (2011).

[18] V. Aravindan, K.B. Jinesh, R.R. Prabhakar, V.S. Kale, S. Madhavi, Atomic layer deposited (ALD) SnO2anodes with exceptional cycleability for Li-ion batteries, Nano Energy. 2 (2013) 720–725. doi:10.1016/j.nanoen.2012.12.007.

[19] B. Ahmed, D.H. Anjum, Y. Gogotsi, H.N. Alshareef, Atomic layer deposition of SnO2on MXene for Li-ion battery anodes, Nano Energy. 34 (2017) 249–256. doi:10.1016/j.nanoen.2017.02.043.

[20] F. Mattelaer, P.M. Vereecken, J. Dendooven, C. Detavernier, Deposition of MnO anode and MnO_2 cathode thin films by plasma enhanced atomic layer deposition using the $Mn(thd)_3$ precursor, Chem. Mater. 27 (2015) 3628–3635. doi:10.1021/acs.chemmater.5b00255.

[21] J. Chae, H.-S. Park, S. Kang, Atomic Layer Deposition of Nickel by the Reduction of Preformed Nickel Oxide, Electrochem. Solid-State Lett. 5 (2002) C64. doi:10.1149/1.1475199.

[22] E. Memarzadeh Lotfabad, P. Kalisvaart, K. Cui, A. Kohandehghan, M. Kupsta, B. Olsen, D. Mitlin, ALD TiO2 coated silicon nanowires for lithium ion battery anodes with enhanced cycling stability and coulombic efficiency, Phys. Chem. Chem. Phys. 15 (2013) 13646. doi:10.1039/c3cp52485j.

[23] E. Østreng, K.B. Gandrud, Y. Hu, O. Nilsen, H. Fjellvåg, High power nano-structured V_2O_5 thin film cathodes by atomic layer deposition, J. Mater. Chem. A. 2 (2014) 15044–15051. doi:10.1039/C4TA00694A.

[24] C. Guan, X. Qian, X. Wang, Y. Cao, Q. Zhang, A. Li, J. Wang, Atomic layer deposition of Co3O4on carbon nanotubes/carbon cloth for high-capacitance and ultrastable supercapacitor electrode, Nanotechnology. 26 (2015). doi:10.1088/0957-4484/26/9/094001.

[25] M.R. Saleem, S. Honkanen, J. Turunen, Thermal properties of TiO_2 films fabricated by atomic layer deposition, IOP Conf. Ser. Mater. Sci. Eng. 60 (2014) 012008. doi:10.1088/1757-899X/60/1/012008.

[26] M. Ara, K. Wadumesthrige, T. Meng, S.O. Salley, K.Y.S. Ng, Effect of microstructure and Sn/C ratio in SnO_2 –graphene nanocomposites for lithium-ion battery performance, RSC Adv. 4 (2014) 20540–20547. doi:10.1039/C4RA00851K.

[27] C.-F. Chen, A. Verma, P.P. Mukherjee, Probing the Role of Electrode Microstructure in the Lithium-Ion Battery Thermal Behavior, J. Electrochem. Soc. 164 (2017) E3146–E3158. doi:10.1149/2.0161711jes.

[28] C.C. Pan, C.E. Banks, W.X. Song, C.W. Wang, Q.Y. Chen, X.B. Ji, Recent development of LiNixCoyMnzO2: Impact of micro/nano structures for imparting improvements in lithium batteries, Trans. Nonferrous Met. Soc. China (English Ed. 23 (2013) 108–119. doi:10.1016/S1003-6326(13)62436-X.

[29] L. Cheng, W. Chen, M. Kunz, K. Persson, N. Tamura, G. Chen, M. Doeff, Effect of surface microstructure on electrochemical performance of garnet solid electrolytes, ACS Appl. Mater. Interfaces. 7 (2015) 2073–2081. doi:10.1021/am508111r.

[30] D.-W. Chung, the Effect of Microstructure on the Performance of Li-Ion Porous Electrodes, (2013).

[31] T.V.S.L. Satyavani, A. Srinivas Kumar, P.S.V. Subba Rao, Methods of synthesis and performance improvement of lithium iron phosphate for high rate Li-ion batteries: A review, Eng. Sci. Technol. an Int. J. 19 (2016) 178–188. doi:10.1016/j.jestch.2015.06.002.

[32] D. Mesguich, J.M. Bassat, C. Aymonier, A. Brüll, L. Dessemond, E. Djurado, Influence of crystallinity and particle size on the electrochemical properties of spray pyrolyzed Nd2NiO4+δpowders, Electrochim. Acta. 87 (2013) 330–335. doi:10.1016/j.electacta.2012.07.134.

[33] L. Ji, Z. Lin, M. Alcoutlabi, X. Zhang, Recent developments in nanostructured anode materials for rechargeable lithium-ion batteries, Energy Environ. Sci. 4 (2011) 2682. doi:10.1039/c0ee00699h.

[34] L. Cong, H. Xie, J. Li, Hierarchical Structures Based on Two-Dimensional Nanomaterials for Rechargeable Lithium Batteries, Adv. Energy Mater. 7 (2017). doi:10.1002/aenm.201601906.

[35] B. Wang, B. Luo, X. Li, L. Zhi, The dimensionality of Sn anodes in Li-ion batteries, Mater. Today. 15 (2012) 544–552. doi:10.1016/S1369-7021(13)70012-9.

[36] N. Nitta, G. Yushin, High-capacity anode materials for lithium-ion batteries: Choice of elements and structures for active particles, Part. Part. Syst. Charact. 31 (2014) 317–336. doi:10.1002/ppsc.201300231.

VITA

Susmita Sarkar was born in Sabroom, Tripura, India. She received her Bachelor of Technology degree in Electronics and Communication Engineering from National Institute of Technology, Agartala, India in 2015.

Susmita joined Missouri University of Science and Technology in August 2015 and held the positions of Graduate Research Assistant and Graduate Teaching Assistant in the department of Mechanical Engineering while working towards her Master of Science degree at Missouri S & T. The degree of Master of Science in Mechanical Engineering was awarded to Susmita in May 2018 from Missouri S & T.